Chapter 5

Trigger Simulations

The inevitable prerequisite for designing any detector or trigger hardware in the high energy physics complicated experiments is the Monte Carlo (MC) simulation.

Trigger studies should answer these basic questions:

1. what are the signatures of the physics process we want to trigger on?
2. what kind of background processes could compete with the physics and what are the signatures of these processes ?
3. what is the considered detector response to the particles entering this detector ?
4. which trigger elements or what trigger logic could be built using the information provided by the detector ?
5. how the different trigger elements from different detectors could be combined and used for the given physics process?
6. what is the trigger efficiency of the different trigger schemes for specific physics classes, what are the corresponding background rates ?

First ideas and hints to answer the above mentioned questions can be obtained from the studies on the 4-vector output from the MC generators. MC generators are used mainly for the first task and partially for the second one, when considering background from other physics processes.

It is however insufficient to simulate complex detector systems and evaluate reliable trigger algorithms within this approach. Simple smearing of 4-vectors is insufficient to reach the required level of precision and sophistication.

The differences in terms of CPU time requirements between the MC event generator and the full detailed detector simulation program are enormous. Therefore various methods are developed to speed up the simulation. Usually $2-3$ different simulation packages, with different level of sophistication, with different precision and proportionaly different CPU time requirements are used. The usage of the certain version is determined by the precision required.

For detector studies a very detailed geometry description and sophisticated tracking of the individual particles is needed. From these kind of studies the absolute response and the resolution of the detector is obtainable. Typical CPU time consumption is of the order of $1s/GeV$ and scales lineary with the particle energy [73].

This approach is not usable for the event simulation for physics analysis (e.g. acceptance calculation, trigger efficiency). The CPU time reduction can be achieved by simplifying the detector geometry description, averaging the detector media properties, and parametrizing the shower developments in the calorimeters or by applying higher cut-offs for particle tracking. All these measures should not deteriorate the precision of the final results, simulation still has to retain the accuracy needed for the studied task.

For the feasibility studies requiring only very limited precision, a strongly simplified detector geometry, parametrization of the showers development and high tracking cut-offs are satisfactory. Within this attitude the speed of $0.1s/100\,GeV$ showers with a logarithmic dependence of the CPU time on the energy was achieved [73].

In the H1 collaboration the following detector simulation programs, with different levels of simplification are used (see Appendix A):

- H1PSI - very coarse detector description, shower parametrization
- H1FAST - averaged calorimeter medium, parametrized shower development, but still detailed simulations in cracks
- H1SIM - detailed detector description, detailed simulation

When comparing CPU time consumption, H1SIM needs e.g. 1000$\times$ more time than the simple MC event generation and H1FAST is $\sim$ 10$\times$ faster than H1SIM [73]. The event processing time of the H1PSI is about 0.06 sec on the IBM 9000/720 and this is gain factor of $\sim$ 500 when compared to the H1FAST time consumption.

5.1 BSET Trigger Design Simulations

The design studies of the electron trigger for the BEMC were limited by the fact that the detector itself was already designed and being completed at DESY. The basic question was how could we use the existing structure to build an efficient electron trigger. Originally the BEMC was proposed to be only as a part of the LAr calorimeter trigger, which in fact did not use the whole potential of this device. The largest defficiency of this proposal was the too coarse granularity of the trigger. The BEMC was divided into eight big towers (1 big tower is defined as a sum from 4 resp. 18 stacks, see Fig. 2.2) and as a final trigger element was considered only the total sum from all BEMC big towers - the total BEMC energy. In the background conditions at HERA, especially in the H1 backward area, this would lead to a high trigger threshold ($E_{tot} \sim 15 - 20\,GeV$) and thus very limited acces to the most interesting NC DIS physics in the kinematical region of *low x, high y.*

Therefore additional design studies with the aim to use the smallest available energy sum - the *stack energy* - were done in the following three steps:

1. The size of the electromagnetic (EM) and hadronic showers in terms of the number of hit stacks and the energy sharing between the adjacent stacks was studied. The longitudinal segmentation of the BEMC stacks was also investigated with the aim to use the so called hadronic part of the stack for electron identification. From these studies we have defined *clusters*, their size and energy thresholds for given electron energies.

2. In the second step we have tried to understand the event topology and characteristics of the physics processes we want to trigger on and also the features of the possible background sources.

3. In the last step we have defined and tuned trigger algorithms and thresholds in order to achieve reasonable trigger efficiencies and simultaneously acceptable rates from all background sources.

5.1.1 Electromagnetic Showers in the BEMC

Radial size of EM showers

This size was studied in the terms of the proposed basic BEMC trigger element - stack energy. We have considered the following questions:

- energy sharing between the hit stacks, energy deposition in the leading stack
- number of hit stacks as a function of the stack thresholds
- energy dependence of the first two parameters
- effect of the expected noise contribution

From the EM cluster size and from the simple geometrical considerations one could expect always at least 1 stack with at least 25% of the total cluster energy. The actual fraction of events with this kind of energy sharing is very small and in most events the leading stack contains $> 50\,\%$ of the cluster energy (Fig. 5.1d). The reason for this is in the interplay of the BEMC non-projectivity in the $\theta - \phi$ plane and the lateral size of electromagnetic showers. From Figs. 5.1b,c we can see the regions hit by $30\,GeV$ electrons in which the leading stack has less than 40% and 50% of the total deposited energy respectively. A clear angular dependence can be seen. At bigger radii the regions with the considered energy sharing are moving from the cracks more to the centers of the hit stacks. These regions are the same as those where the energy losses in the cracks between stacks are important and where the largest energy corrections have to be applied to the measured energy [77].

From the energy sharing between the stacks and from the fraction of energy deposited in the leading stack, i.e. in the stack with maximal energy deposit, we have defined **stack high thresholds (HT)** as a seed for the trigger cluster. Fractions of the total cluster energy detected in the leading stack are very similar for the whole electron energy spectrum. An example for 30 GeV electrons is shown in Fig. 5.1(d). The general rule outcoming from these studies is that stack HT should be set to $\sim 30-40\%$ of the electron energy we want to trigger on (Fig. 5.2). It means e.g. that with the stack $HT = 3\,GeV$ we will safely trigger on $E_e > 10\,GeV$. We will trigger also on most of the electrons $E_e > 5\,GeV$, but here some fraction of events could be lost already due to the HT value. This should be kept in mind when setting the trigger thresholds.

In principle we could trigger on the simple requirement of the stack energy above HT. But this simple condition is not acceptable due to the high background rate. We need higher thresholds but still to be able to trigger on low energy electrons. This dilemma can be solved by summing up energy depositions also from stacks surrounding the leading

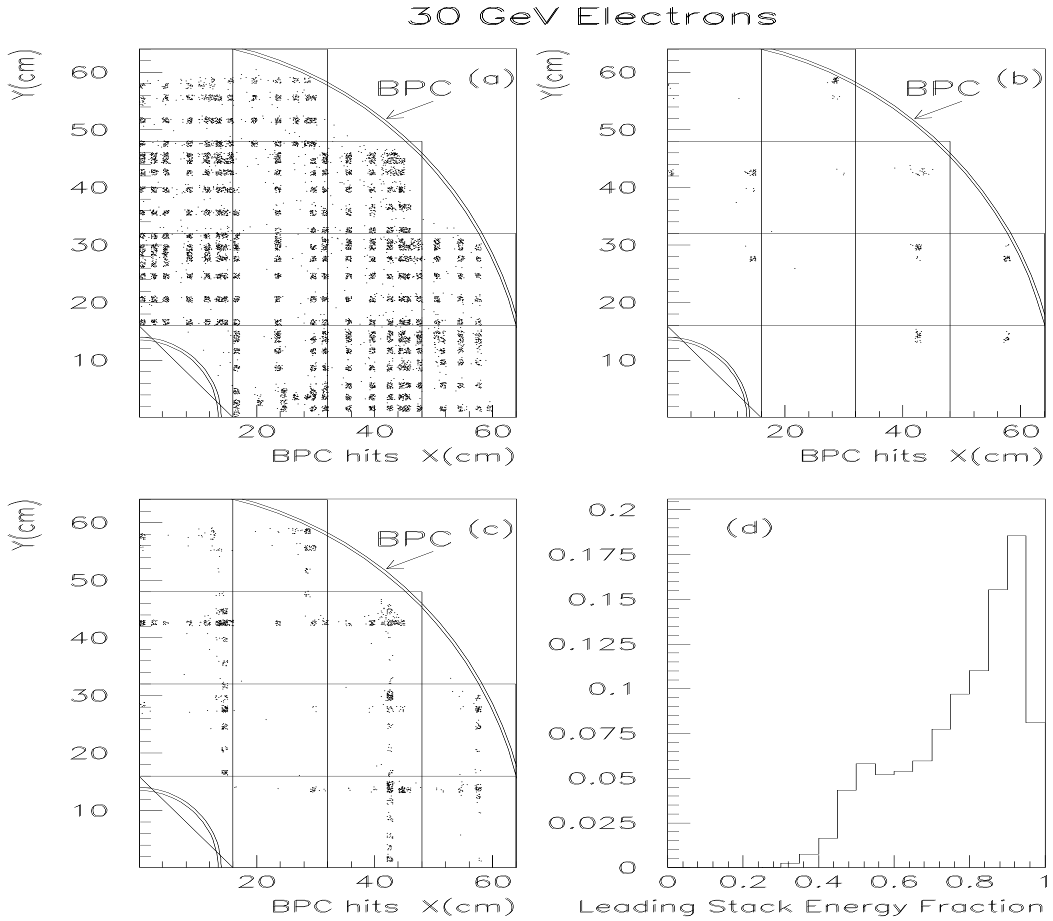

Figure 5.1: *Simulation of 30 GeV electrons hitting BPC and BEMC under realistic angles for part of the detectors quadrant. Shown are BPC hits coordinates and the BEMC stacks: (a) all events; (b), (c) only events in which energy in the leading stack was* $< 40\%$*, resp.* $< 50\%$ *of the cluster energy; (d) Cluster energy fraction in the leading stack for all simulated events.*

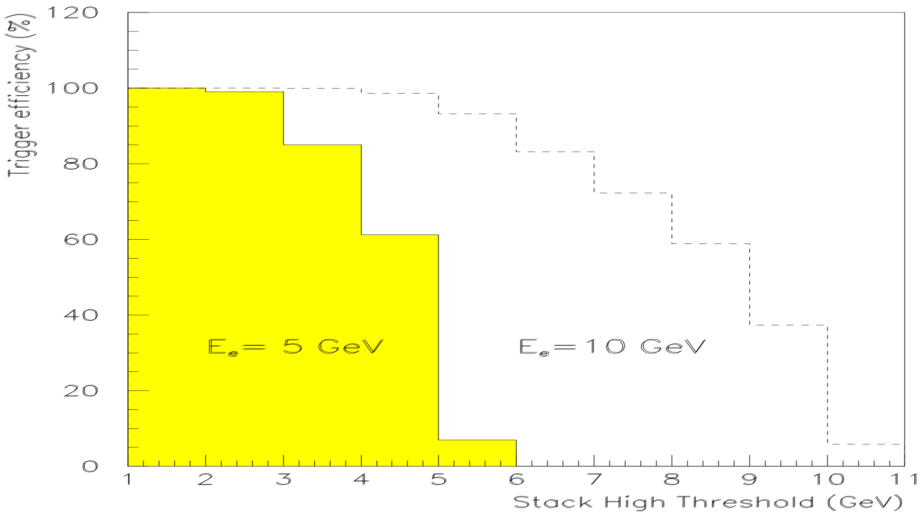

Figure 5.2: *The effect of the stack high threshold values (HT) on the trigger efficiency for 5 and 10 GeV electrons. No low thresholds and no cluster thresholds are applied. At least 80% of the incident energy is required to be deposited in the detector.*

stack. For this purpose we have defined the so-called **low thresholds** LT. LTs enable contribution to the BEMC **total trigger energy** ($BTOT$) and to the **trigger cluster energy** ($TCLUS$). $TCLUS$ is built only in the case that there exists at least 1 stack above HT, i.e. HT works as a $TCLUS$ initiator. Neighbouring stacks above LT are contributing to the trigger cluster energy sum. In order to have a good correlation between the trigger cluster and the real cluster, the LT should be as low as possible. The lower the LT, the better the correlation between real cluster and the trigger cluster. These LTs are set to 3-4 σ above the noise level (called also noise thresholds).

Distributions of the number of hit stacks at four stack thresholds 0.4, 0.7, 1.1, and $2.0\,GeV$ for electron beam energy $30\,GeV$ are shown on the Fig. 5.3. From this detailed MC simulation with H1SIM we see that down to the stack threshold of $\sim 1.0\,GeV$ the maximal number of stacks found above this threshold is 4. This is valid for all electron energies up to the maximal electron beam energy 30 GeV which is designed for HERA. This result provides us the **trigger cluster** definition as a **group of** 2×2 **adjacent stacks** above the defined threshold. Only below $\sim 1.0\,GeV$ there is some small probability to have more than 4 stacks in the cluster and in this case the proper trigger cluster definition would be 3×3 stacks.

Longitudinal size of EM showers

The longitudinal shape of the electromagnetic showers can be measured from two samplings: from energy deposit along the whole stack and from the energy detected in the last third of the stack ("hadronic" section). The fraction of the total cluster energy leaking into this hadronic part ($R = E_{back}/E_{clus}$) was considered as a potential trigger element,

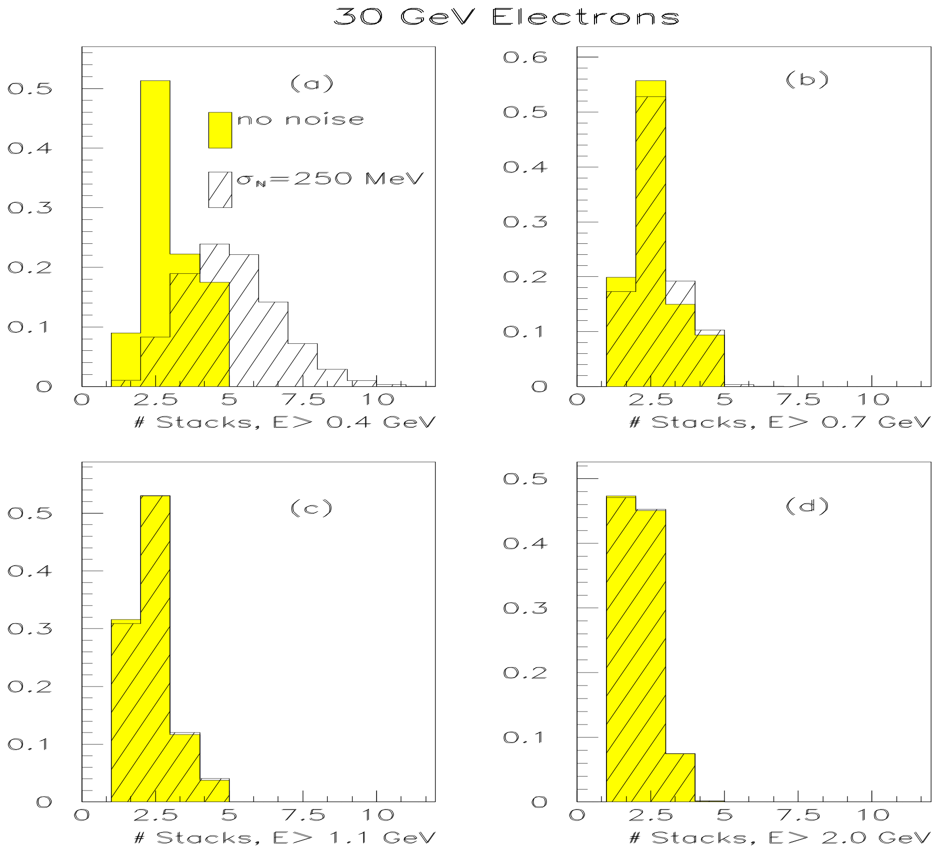

Figure 5.3: *Simulation of 30 GeV electrons hitting BPC and BEMC under realistic angles without and with expected noise contribution* $\sigma = 250\, MeV$ *per stack. Shown are number of hit stacks with energies above defined stack thresholds. The content of the histograms is normalized to 1.*

which could work as a veto against the HERA machine induced background and simultaneously as a tool distinguishing electrons from hadrons originating in the interaction region. Electromagnetic showers in the BEMC are rather short and in $> 99\%$ of cases the leakage R is smaller than 0.2. But fluctuations in the shower development, mainly in the crack regions, create tails reaching $R \sim 0.6$ (Fig. 5.4).

From the longitudinal shape of the electromagnetic showers only, the energy fraction value $R > 0.2 - 0.3$ can be considered as a potential veto trigger element against all kinds of background competing with electron identification.

BEMC Angular Acceptance

The trigger efficiency can be strongly affected by the energy leakage out of the detector. Leakage problems arise at angles above 173^0 (close to the beam pipe) where electrons hit the BEMC near to the edge and the part of energy is lost due to the transversal size of the shower. Due to the triangular form of the innermost BEMC stacks the energy losses

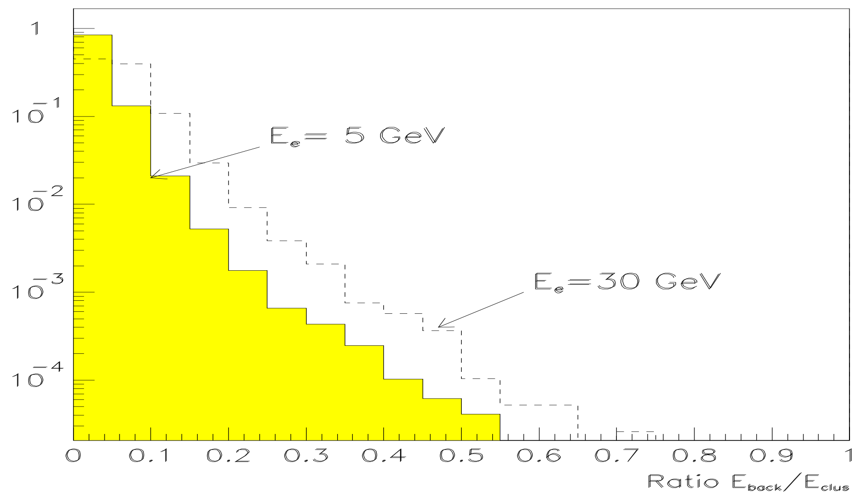

Figure 5.4: *Longitudinal shape of 5 and 30 GeV electromagnetic showers in the terms of the energy ratio* $R = E_{back}/E_{clus}$. *Only events with energy deposit of* $>$ 80% *from the incident particle energy are considered.*

are also dependent on the azimuthal angle ϕ (Fig. 2.2).

The second area with leakage problems appears at angles smaller than 156^0 (Fig. 2.3). In this case BEMC depth seen by the traversing particle is not sufficient for full containment and since the geometry is not projective, the side leakage also plays an important role. Overlap with the liquid argon calorimeter is not very good and large energy corrections should be applied in this region.

Other areas where some fraction of the energy is lost, even in the good angular region, are in between the BEMC stacks, in the so called cracks.

5.1.2 Hadronic Showers in the BEMC

The BEMC with a total depth of $1\,\lambda$ is very short for the full manifestation of the typical properties of hadronic showers which are usually needed to separate them from EM showers. More than 1/3 of all hadrons pass through the BEMC as a minimum ionizing particles and produce a typical peak at few hundred MeV (Fig. 5.5a). This means that they are invisible to the trigger. The rest of hadrons deposit more energy but with big fluctuations, causing large tails in the visible energy spectrum. Trigger efficiency for these kind of events is very small. Nevertheless this small efficiency is compensated by the high rates from photoproduction processes and therefore it is useful to separate electrons from hadrons already on the trigger level. Taking into account noise and thresholds there is no difference in the lateral size of EM and hadronic showers. Only the longitudinal size of the showers, expressed via parameter $R = E_{back}/E_{clus}$, is of some use (Fig. 5.5b) for e^-/h separation. With condition $R < 0.1$ the hadronic rates could be suppressed by a factor $2-4$. From the shapes of EM showers the $R < 0.3 - 0.4$ values are desirable. But then the achieved hadrons rate suppresion factor is very small (< 2) and therefore the usage of R parameter in the trigger is doubtfull. The final decision will be made only after studies of the efficiency of the suppresion of beam induced background.

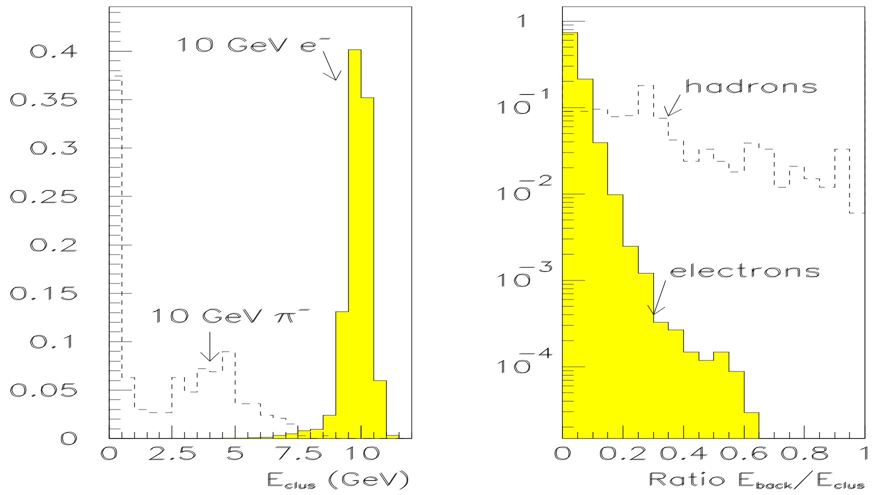

Figure 5.5: *(a) Energy spectra of 10 GeV π^- and e^-. (b) A first look at the parameter R for the same particles is rather promising for e^-/π separation. But taking into account stack thresholds determined by the noise conditions, the achieved reduction of trigger rates is very small.*

5.1.3 NC DIS and Photoproduction Events in the BEMC

Topology of the NC DIS in the BEMC

For NC DIS events topology studies in the BEMC mainly DJANGO MC generator was used [65]. DJANGO is an interface written in order to merge two stand alone MC generators: HERACLES [66], simulating electroweak processes with included first order radiative corrections, and LEPTO [67] for the subsequent simulation of QCD processes and fragmentation. MC generator studies indicate that the rate of hadrons and photons from the hadronic final state hitting BEMC together with the scattered electron starts to be comparable to that of electron itself only below $E_e \sim 8\,GeV$ (Fig. 5.6). In the table 5.1 the fractions of events with an additional particle in the BEMC are shown for different E_e bins and different MC generators. In the kinematical peak region ($E_e > 22\,GeV$) only $4 - 12\,\%$ of events have an another particle hitting the BEMC. The mean energy of these particles is $\sim 1\,GeV$ and the maximal energy limit $4.7\,GeV$ follows from the kinematics. The typical signature of these events will be therefore 1 high energy cluster in the BEMC.

Events in the kinematical peak are used for the absolute energy scale determination. But from the physics point of view, more interesting are events at higher y, i.e. at $E_e < 22\,GeV$. The smaller the E_e the higher the probability of having another particles in the

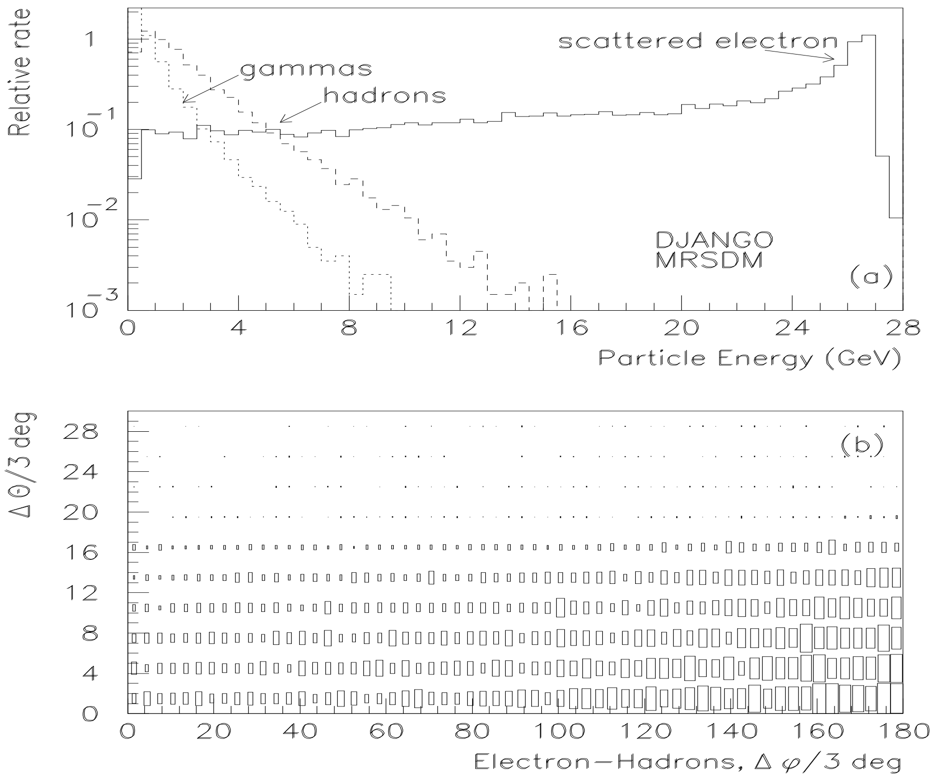

Figure 5.6: *(a) Relative rates of electron and other particles hitting BEMC as a function of particles energy; (b) Angular separation, 3°/bin, between electron and hadrons hitting BEMC.*

BEMC and the higher is also multplicity and the maximal possible energy of these particles. On the Fig. 5.7 is shown the particles multiplicity distribution and resulting number of stacks found above HT resp. LT. The distributions are for two kinematical regions when the scattered electron energy in the BEMC is $> 10\,GeV$ resp. $4\,GeV < E_e < 10\,GeV$.

Mean multiplicities and energy spectra of these electron "companions" are of course dependent on the fragmentation and hadronization schemes used in the different MC generators.

From the studies of electron angular separation from other particles hitting BEMC, it follows that electron appears rather isolated and accompanying particles tend to be scattered at the same polar angle θ but back to back in azimuthal angle ϕ (Fig. 5.6). The probability of hitting the same stack as electron is negligible ($< 1\%$), and the probability of having another particle in the cluster of the size 3×3 stacks is still rather small $\sim 3.5\%$.

For the trigger the consequences are clear: one has to consider the possibility of the existence of more energy clusters in the BEMC. With very high probability the electron will produce cluster with the highest energy (*leading cluster*) and photons and/or hadrons

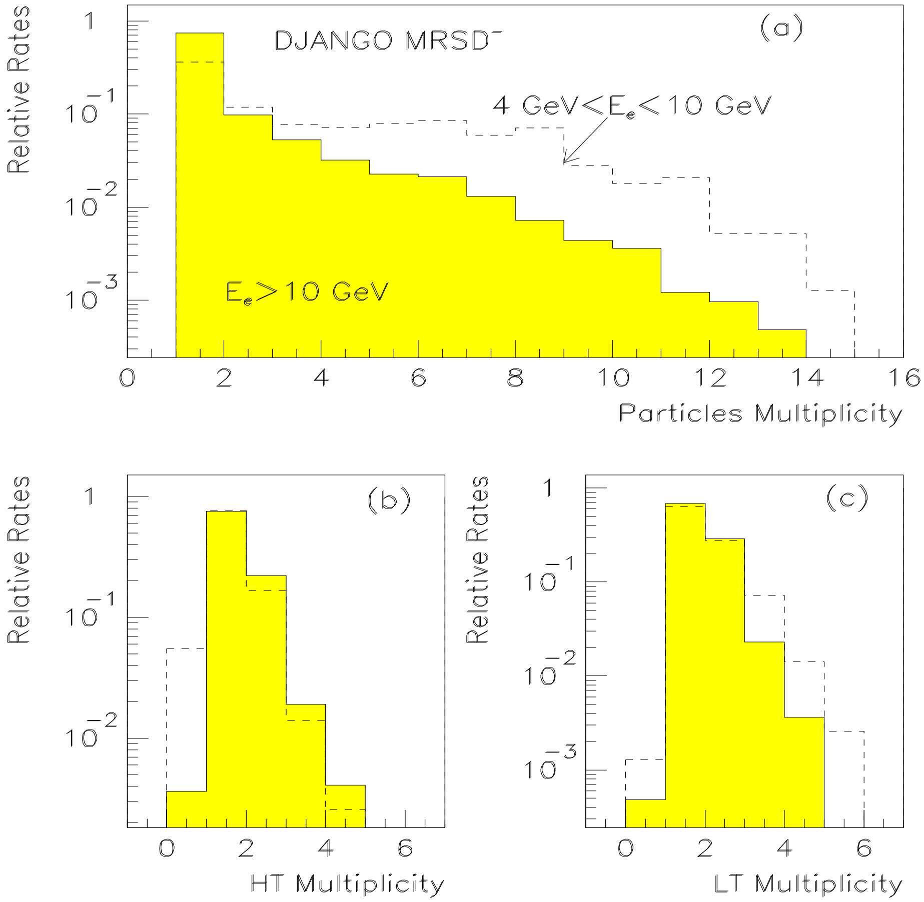

Figure 5.7: *(a) Number of particles hitting the BEMC (with electron) for two different kinematical regions and corresponding number of stacks above 2.3 GeV (b) resp. 1.3 GeV (c).*

particles	MC generator	$E_e\,(GeV)$			
		< 10	$10 - 15$	$15 - 22$	> 22
any particle	LEPTO	0.99	0.99	0.80	0.12
	DJANGO	0.63	0.63	0.42	0.04
hadrons	LEPTO	0.97	0.95	0.68	0.06
	DJANGO	0.56	0.55	0.32	0.02
gammas	LEPTO	0.85	0.77	0.52	0.07
	DJANGO	0.51	0.44	0.25	0.02

Table 5.1: *Fraction of events with additional particles in BEMC for different scattered electron energies. The difference between two generators is in this case due to the electroweak radiative corrections applied in the DJANGO. It means that effective energy of the initial electron beam is smaller.*

can produce additional clusters of smaller energies. Number of these clusters seen also by the trigger depends on the thresholds setting. Our goal is to trigger on the electrons down to $4 - 6\,GeV$ and this means that stack high threshold must be $\sim 2 - 3\,GeV$. Differences in trigger efficiencies, when requiring exactly 1 trigger cluster ($EQ1$) or admitting also more ($GE1$) are shown on the Fig. 5.9a,b. The fraction of events with more than 1 trigger cluster is small, but the losses due to the requirement of only 1 cluster would introduce trigger bias into the most interesting kinematical region. Any exact cluster counting is not applicable for BEMC for many reasons:

- particles multiplicity hitting BEMC depends on the hadronization which is unknown and the subject of different model predictions
- limited BEMC angular acceptance
- BEMC is only an electromagnetic calorimeter with a bad hadronic energy measurement

Therefore only the most simple information about the cluster multiplicity can be used in the trigger:

- exactly 1 cluster has been identified ($EQ1$)
- 1 or more clusters were found ($GE1$)

Trigger element EQ1 could be used in the kinematical peak region, where the hadronic contribution to the trigger signal is negligible and on the other hand it could help at the background rejection. Trigger element $GE1$ is safe in the whole kinematical region.

Photoproduction in the BEMC

Photoproduction procceses (γp) are interactions of quasi real photons ($Q^2 \rightarrow 0$) with the proton [69]. Due to very low momentum transfer Q^2 the electron remains in the beam pipe and takes away a large fraction of the total available energy (26.7 GeV). Therefore only hadrons and/or overlaping γ/h could mimic the electron.

For the generation of the photoproduction events we have used two MC programs: PYTHIA [70] (for hard scattering) and RAYVDM [71] (for soft procceses). The energy spectrum of the particles from the γp interactions hitting the BEMC has a peak at $\sim 1\,GeV$ and tails reach up to $12-15\,GeV$. As a result of their high cross section these events could be a serious source of background for NC DIS trigger at $y > 0.7$. Although the scattered electron from NC DIS will be isolated and the fake 'electron' from γp interaction will be mostly accompanied by other particles, this feature is not usable in the trigger, due to the low energy of γp produced particles. After applying realistic stack thresholds all differences in the event topologies escape and are not projected nor into the cluster size, nor into the total number of stacks above LT or HT. To get rid of the photoproduction background is a big problem even for the off line physics analysis, where information from the whole H1 detector is available. The expected contribution to the NC DIS BSET trigger rates at the design luminosity depends on the thresholds and e.g for CL1=4 GeV it could reach a few Hz.

5.1.4 Machine Background Simulations

The background event rate from the HERA machine is expected to be five orders of magnitude larger than that from NC DIS. It is necessary to study the signatures of the background events and to find effective algorithms to reduce their rates to the acceptable level. The main background load is delivered to the detectors close to the beam pipe : Plug, IF part of the LAr calorimeter and BEMC. Tails of the energy deposits reach a few hundred GeV. It is clear that these are the most difficult trigger areas of the H1 detector. Of course also tracking detectors suffer, mainly because they are sensitive down to energies of a few 100 MeV. Tracks pointing outside the H1 detector are a clear signature for this kind of background (Fig. 4.1).

The problematic region of the LAr calorimeter is expected to be the inner forward (IF) part, where the energy thresholds have to be set much higher than in the rest of the calorimeter. The thresholds in the forward and central barrel part (FB, CB) are not determined by the background energies but rather by the noise level of the calorimeter.

In further studies we will concentrate on the BEMC as the main detector for measuring and triggering electrons scattered with low Q^2, x values. Triggering in this area is difficult because the background energy spectrum covers the whole physics energy spectrum and with much higher rates (Table 5.2, 5.3).

Beam-Gas Simulations Beam-gas interactions are simulated in three steps, with three different MC packages: MODC (modified cluster generator), BEAMLINE and H1SIM.

MODC [49] is an empirical MC simulation package, i.e. it is a mixture of some basic physics ideas on hadron-hadron collisions tuned to the UA5 experimental data. The primary interaction of the proton beam with the HERA rest gas molecules, which can take place starting at $z \simeq -80\ m$, is simulated by the MODC and further transport of secondaries as well as tracking up to this interaction point is made by the BEAMLINE simulation program. For the simulation of secondary hadronic interactions with the beam pipe the standard GHEISHA module in the framework of the GEANT simulation package is used. There are no secondary beam-gas interactions. At $z = -3.37\,m$ H1SIM takes over the 4-vectors of produced particles, which are stored in the standard BOS banks by the MODC+BEAMLINE programs. Then the simulation in the H1 detector itself follows [79].

The beam-gas events (BGE) which originate in the interaction region are most difficult to be recognized. The histograming technique used by the $ZVTX$ trigger in coincidence with veto from TOF reduces the rate to few hundred Hz or less. This is still too much and additional subtriggers are put into the coincidence such as e.g. $DC - r\phi$ and/or BSET trigger.

Beam-Wall Simulations Beam-wall events (BWE) rate is determined mainly by the proton beam life time. Usually the values between 10-40 hours are considered. Very important is also the efficiency of the collimators (scrapers) in the straight sections of the HERA ring, which are supposed to reduce the off-momentum proton flux by factor ~ 100. It means that already from this very first simple considerations any BWE rate calculation starts with an uncertainty factor of ≥ 4. Final decisive element influencing the BWE rate is the beam pipe geometry and geometry of the quadrupole magnets QS $\simeq 40\,m$ in front of the H1 detector [79].

BWE generation begins therefore at the QS magnets, where the hadronic interactions of the $820\,GeV$ protons are simulated with GEISHA or FLUKA programs. Products of these interactions are further transported over 36 m by the BEAMLINE program. At the same point as in the case of BGE simulations ($z = -3.37\,m$) H1SIM program takes over all particles produced in both previous steps and from this moment further secondary interactions in the volume of H1 detector can occur [79].

Background Events in BEMC

BEMC is the first major detector hit by the proton induced background and the trigger is exposed to very high rates and large energy depositions. Typical rates and energy spectra per stack as a function of radial distance from the beam axis (stacks are grouped into so called rings) are shown on the Fig. 5.8. Effective separation of the physics and background signals mainly in the innermost part of the detector, closest to the beam pipe, is a big challenge.

Off-momentum protons interact with the different elements in and/or with the beam pipe itself and produce hadronic showers. Large fraction ($> 98\%$) of these events depositing energy in the BEMC will be tagged by the TOF veto counter ($\overline{TOF}$) and thus can be rejected at L1. But even the remaining 2% means a trigger rate of the order of few hundred Hz. Unfortunately, an ion getter pump (at $z = -2.06; -2.24\,m$) and a synchrotron radiation mask (at $z = -1.7\,m$) are placed directly between the TOF scintillator planes in the beam pipe and under the BEMC resp. Background events originating at these scatter sources cannot be vetoed by the coincidence signal from both TOF planes. A looser trigger condition requiring a veto signal only from one TOF plane ($\overline{TOF1}$), closer to the BEMC, reduces the rate by additional factor $\sim 3-4$.

As the highest rates with biggest energies are coming from the 4 innermost triangular stacks, we have tried to treat them separately. First we have excluded them from the trigger as a possible cluster initiators (I_{out}), i.e. HT was set to $> 100\,GeV$. But low thresholds are treated the same way as other stacks, i.e. they are allowed to contribute to the energy sums.

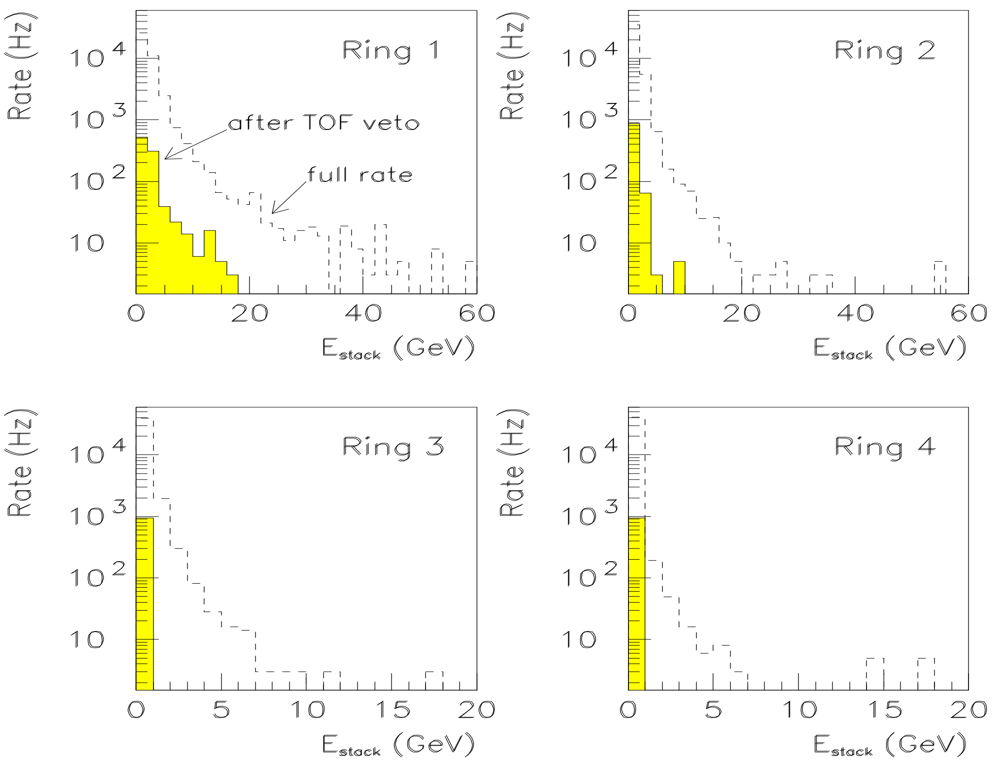

Figure 5.8: *Radial dependance of rates and energy spectra for individual stacks grouped into so called rings. Highest rates and biggest energies are deposited in the innermost ring 1. TOF veto is very effective mainly for outer rings 3 and 4.*

This operation alone helped to reduce the background rate by factor $\sim 3-10$ depending on the trigger element considered. A less severe condition of setting HT at $10\,GeV$ (I_{10}) brought also a small improvement and we have thus achieved a rate reduction by a factor ≤ 2. This trigger condition is meant for triggering of electrons in the kinematical peak ($E_e > 22\,GeV$) and enabling thus in situ calibration of the triangular stacks. For these kind of events we can require only one of these innermost stacks to be above HT. This brings another factor ~ 2 into the background rejection. Another possibility is to set also other stacks to different HT - so called ring dependent thresholds could be used. The closer the stack to the beam axis, the higher its HT. But due to the bad $r-\phi$ symmetry of the BEMC stacks, this threshold setting would complicate the off-line trigger acceptance calculation. Typical rates expected from the BSET trigger elements itself and put into coincidence with TOF and/or special treatment of the innermost triangular stacks are shown in the Table 5.2.

Another potential trigger element mentioned in the studies of longitudinal shape of the showers, namely the ratio $R = E_{BACK}/E_{CLUST}$, brings only very small rejection of the events triggered by GE1, CL1, CL2, CL3 or BTOT. The rejection factor depends on the LT. The lower the LT could be set the better rejection achieved. But at realistic $LT \sim 1.0\,GeV$ and at $R < 0.3$ the achieved reduction by factor ~ 1.1 is not attractive enough to be realized in the hardware. Even at $LT = 0.5\,GeV$ and $R < 0.2$ maximal reduction achieved was only ~ 1.5. Main reason for this small effectivity is the fact that innermost triangular stacks, where the background energy is concentrated, have no hadronic part and thus the ratio for these events is $R = 0$.

Up to now we have considered only the BSET trigger itself (with an inevitable $\overline{TOF}$) and we have found that triggering down to the cluster thresholds of $6 - 8\,GeV$ is possible, i.e. background rates are acceptable even at full design luminosity. But triggering at smaller energies will be a bigger problem and more stringent conditions must be used. For this purpose the coincidence with other subdetectors is required.

The TOF detector provides also TOF-IA (interaction window) signal tagging events from the interaction region. In the ideal case there should be no background events with this trigger bit.

Another direct neighbour is the BPC providing only simple information yes/no about hits in 3 out of 4 wire planes (BPC-S). There is no spatial information available on L1 which could be correlated with the BEMC cluster. Therefore this trigger coincidence is not very powerful and another shortcoming is that BPC does not cover the whole BEMC.

In the simulation we have tested matching of the BEMC stack above HT with the BPC hit wires (BPC-M) [1]. For this purpose we have groupped 16 wires into 1 readout unit called strip. This way we have obtained 20 strips per plane, each of 8 cm width. For stacks above HT the corresponding, matching strips in 3 out of 4 planes were looked for. Matching requirement strongly reduces the BSET trigger rates as can be seen from the Table 5.3-column BPC.

Central tracking detectors as CJC and MWPC are much more effective in the coincidence with BSET as BPC-S and are comparable with BPC-M.

The summary of expected bacground rates from the BSET trigger elements combined with tracking triggers is shown in the Table 5.3.

5.1.5 Proposed BEMC Electron Trigger Elements: Summary

As seen before the basic trigger element is a stack energy and for each stack two thresholds are defined, ***LT*** enabling contribution the the energy sums, and the ***HT*** used as a high energy cluster initiator. Notion of the high energy cluster arose from the fact that the size of the electromagnetic showers is limited to a few adjacent stacks. The groups of hot stacks - **clusters** - are found from the 2-dimensional [X,Y] projections. With this procedure only a limited cluster counting precision is achievable ($EQ1$, $GE1$), but as shown before there is no use of exact cluster multiplicities counting. Cluster search is done simultaneously on both threshold planes, i.e. between stacks above LT as well as between stacks above HT.

The proposed BSET trigger elements used in the simulations to define more efficient trigger algorithm for NC DIS are:

- number of clusters in the low threshold plane

[1] In the meantime realized also in the hardware and prepared to be used on the L3 trigger level.

BSET $*TE$	BSET Triggers Rates (Hz)							
	EQ1	**GE1**	**BTOT**	**CL1**	**CL2**	**CL3**	**LTOR**	**IST**
BWE	9720	18115	17755	14470	11420	5120	25770	14865
BGE	6741	8532	7257	5280	3402	750	15747	6465
$\overline{\textbf{TOF}}*$								
BWE	200	225	105	90	60	15	460	205
BGE	186	192	96	51	54	9	480	174
$\overline{\textbf{TOF1}}*$								
BWE	60	60	15	15	10	5	110	55
BGE	60	60	33	30	24	0	129	48
$\mathbf{I_{10}}*$								
BWE	8345	11700	17755	10155	8450	3970	25770	1245
BGE	3588	4029	7257	2811	2049	534	15747	447
$\mathbf{I_{10}} * \overline{\textbf{TOF}}*$								
BWE	45	50	105	30	25	15	460	20
BGE	39	42	96	30	30	6	480	15
$\mathbf{I_{10}} * \overline{\textbf{TOF1}}*$								
BWE	15	15	15	10	10	5	110	10
BGE	19	15	33	6	6	0	129	3
$\mathbf{I_{out}}*$								
BWE	2920	3250	17755	2140	1135	185	25747	0
BGE	1932	2067	7257	1014	483	48	15747	0
$\mathbf{I_{out}} * \overline{\textbf{TOF}}*$								
BWE	20	20	105	5	0	0	460	0
BGE	18	18	96	6	6	6	480	0
$\mathbf{I_{out}} * \overline{\textbf{TOF1}}*$								
BWE	0	10	15	0	0	0	110	0
BGE	12	12	33	3	3	0	129	0

Table 5.2: *Trigger rates from beam-wall (BWE) and beam-gas (BGE) background events for BSET trigger elements alone and put into coincidence with vetos from TOF and/or special treatment of the innermost stacks (I_{out} - excluded completely, I_{10} - HT=10 GeV). Cluster and total energy thresholds CL1, CL2, CL3, BTOT are 4, 7, 15 and 4 GeV respectively. Stack thresholds are $HT = 2.3\,GeV$ and $LT = 1.3\,GeV$.*

	Combined Triggers Rates (Hz)						
$BSET*$	**ZVTX**		$\mathbf{DC-R\phi}$	**BPC**		**FWR**	**Tracks**
	$\mathbf{-t_0}$	**−sig1**	**−thr0**	−S	−M	$\mathbf{-t_0}$	$\mathbf{-t_0}$
$\mathbf{GE1 * \overline{TOF}*}$							
BWE	80	25	40	195	45	70	90
BGE	81	15	30	156	12	66	102
$\mathbf{GE1 * \overline{TOF1}*}$							
BWE	25	10	15	50	0	20	25
BGE	30	6	15	51	3	24	36
$\mathbf{GE1 * I_{10} * \overline{TOF}*}$							
BWE	15	5	10	45	0	15	15
BGE	81	15	36	156	12	66	112
$\mathbf{GE1 * I_{out} * \overline{TOF}*}$							
BWE	5	0	5	20	0	5	5
BGE	3	3	3	18	0	3	3
$\mathbf{CL1 * \overline{TOF}*}$							
BWE	45	10	15	85	25	30	45
BGE	39	12	15	63	3	30	45
$\mathbf{CL1 * \overline{TOF1}*}$							
BWE	10	5	0	15	0	5	10
BGE	18	6	9	24	0	15	18
$\mathbf{CL1 * I_{10} * \overline{TOF}*}$							
BWE	10	5	5	25	0	10	10
BGE	39	12	15	63	3	30	45
$\mathbf{CL1 * I_{out} * \overline{TOF}*}$							
BWE	0	0	0	5	0	0	0
BGE	3	3	0	6	0	3	3
$\mathbf{BTOT * \overline{TOF}*}$							
BWE	55	10	25	90	-	40	60
BGE	48	15	18	78	-	42	57
$\mathbf{BTOT * \overline{TOF1}*}$							
BWE	10	5	0	15	-	5	10
BGE	18	6	9	27	-	18	21

Table 5.3: *Trigger rates from beam-wall (BWE) and beam-gas (BGE) background events for BSET trigger elements GE1, CL1 and BTOT put into coicidence with different tracker triggers. BPC is shown for standard mode (S) and mode requiring matching stack above HT in BSET (M).* $Tracks - t_0$ *is OR'd from ZVTX-, forward ray (FWR) and CJC* t_0*. Meaning of the TOF vetos and values of BSET thresholds are the same as in the previous table.*

- number of clusters in the high threshold plane (***EQ*1, *GE*1**)
- three cluster energy sums (***CL*1, *CL*2, *CL*3**)
- BEMC total energy (***BTOT***)
- number of hits above HT in the innermost stacks (***IST***)
- at least 1 stack above LT (***LTOR***)

5.2 Trigger Algorithms for NC DIS

5.2.1 Low Q^2 Events

The BEMC detector and trigger are vital for the NC DIS at low Q^2. The main task of the trigger on L1 is to reduce high background rate below 100 Hz and still retain high efficiency for NC DIS events. From the trigger point of view we have found three regions in the BEMC angular acceptance (Fig. 1.2) with different levels of difficulties:

1. *low y* region	- electron energy $E_e > 10\,GeV$, relatively small problems with trigger algorithm and rates
2. $low\,x - high\,y$ region	- $E_e < 10\,GeV$, problems with background rates
3. *large* θ_e region	- problems with background rates and energy leakage for both previous y regions

Low y Trigger

When considering electron energies above $\sim 10-15\,GeV$ the rates from the BSET cluster trigger are reasonable and efficiency for the NC DIS is very high. Cluster trigger CL3 with $E_{th} = 15\,GeV$ can be used as a kinematic peak trigger (Fig. 5.9) and as a trigger monitoring the TOF performance.

But this kinematical region is not the most interesting one, although very useful for the determination of the BEMC absolute energy scale.

Low x - High y Trigger

The more interesting $low\,x - high\,y$ region, where signatures of new physics are expected, will be covered by GE1, CL1, CL2 and BTOT trigger elements (Fig. 5.9). But running with lower calorimeter thresholds means immediate increase of the background rates. Nevertheless in the first period of HERA operation at only $\sim 1\%$ of the design luminosity, it should be possible to run CL2 trigger stand alone at rather low thresholds ($3-4\,GeV$) due to the fact that also background rates are expected to be 2 orders of magnitude smaller.[2]

At full design luminosity the minimal trigger cluster threshold value at which it is aimed to run the stand alone BSET trigger CL2 is $6-8\,GeV$. This would mean $> 90\,\%$ trigger efficiency for $8-10\,GeV$ electrons. Therefore the calorimeter CL2 trigger alone gives a rather poor efficiency for $y > 0.6$ (Fig. 5.11). To trigger electrons below 8-10 GeV

[2] It was really the case, see Chapter 7.

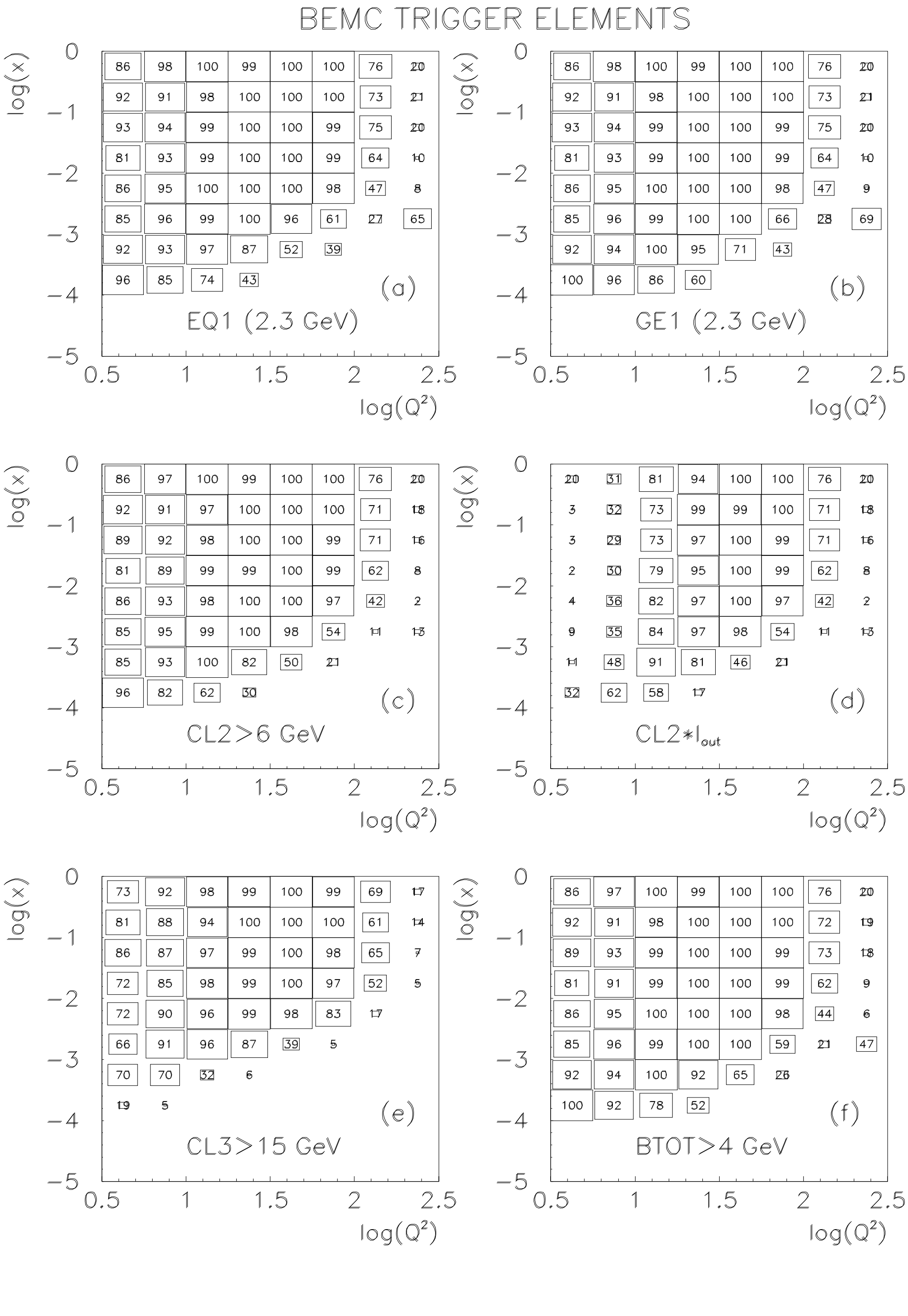

Figure 5.9: *Trigger acceptance of BSET trigger elements for events generated flat in* $\log(Q^2)$*-*$\log(x)$ *plane according the* $MRSD^-$ *distribution from LEPTO 6.1.* (a)-(b) *Importance of the* $GE1$ *condition at high* y *when compared to EQ1.* (c)-(d) *The effect of excluding the innermost stacks from the cluster trigger is shown for* $CL2$*. Cluster trigger threshold values clearly affect efficiency in the whole BEMC for high* y *region and independently from* y *at the BEMC inner and outer borders (b)-(f).*

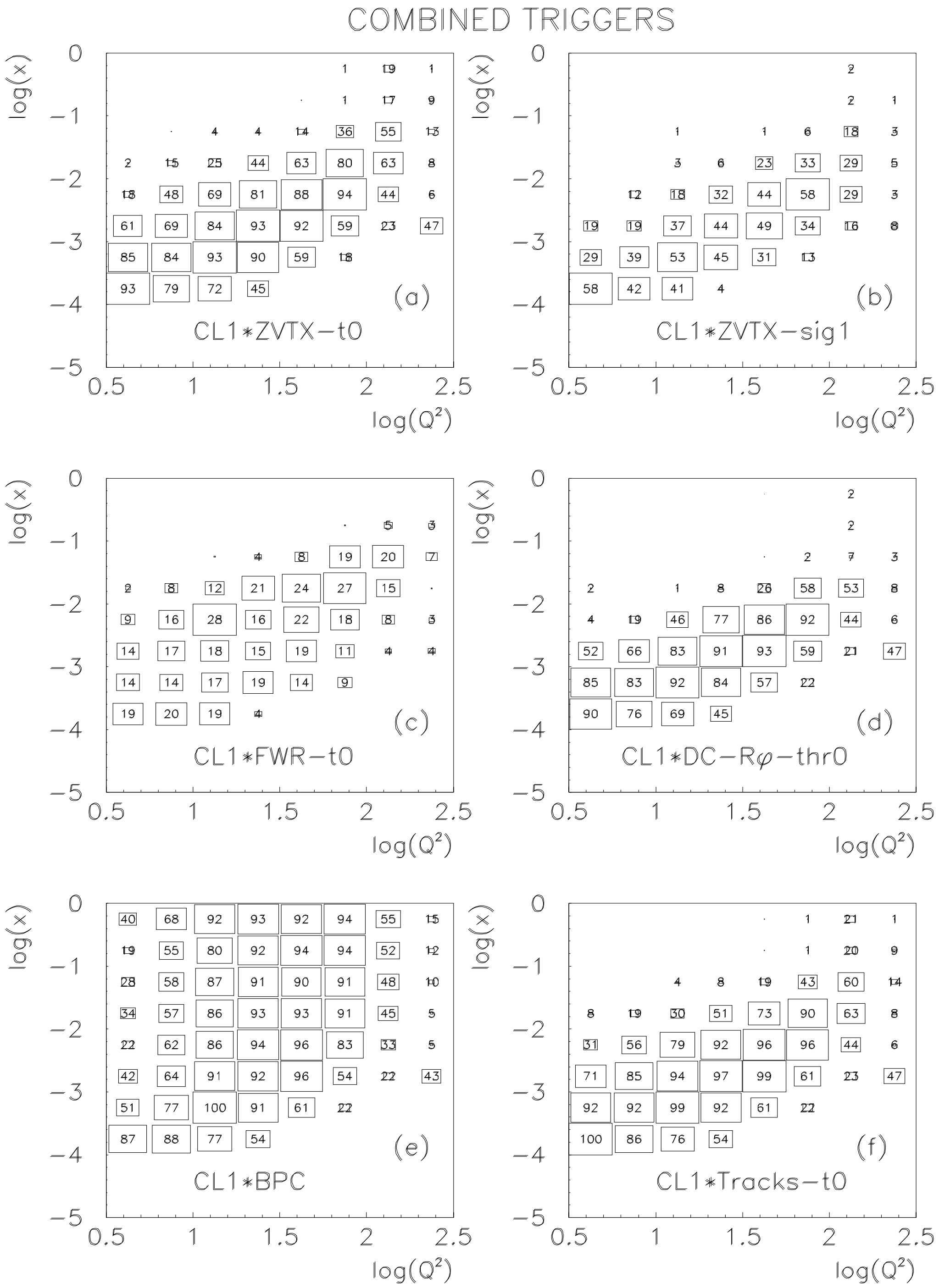

Figure 5.10: *Trigger acceptance of the BSET CL1 trigger (> 4 GeV) in coincidence with tracker triggers.*

the CL1 cluster trigger threshold must be set to 4-5 GeV. Also GE1 at 2-3 GeV could be considered, but both of course only in coincidence with other triggers. Another possibility is to run CL1, GE1 also stand alone but with the so called prescaling. This means that according the prescale factor n only each n^{th} trigger would be accepted. This mode of operation is acceptable only if the prescale factor is not too big allowing accumulation of reasonable amount of the data. The possible triggers are briefly discussed hereafter.

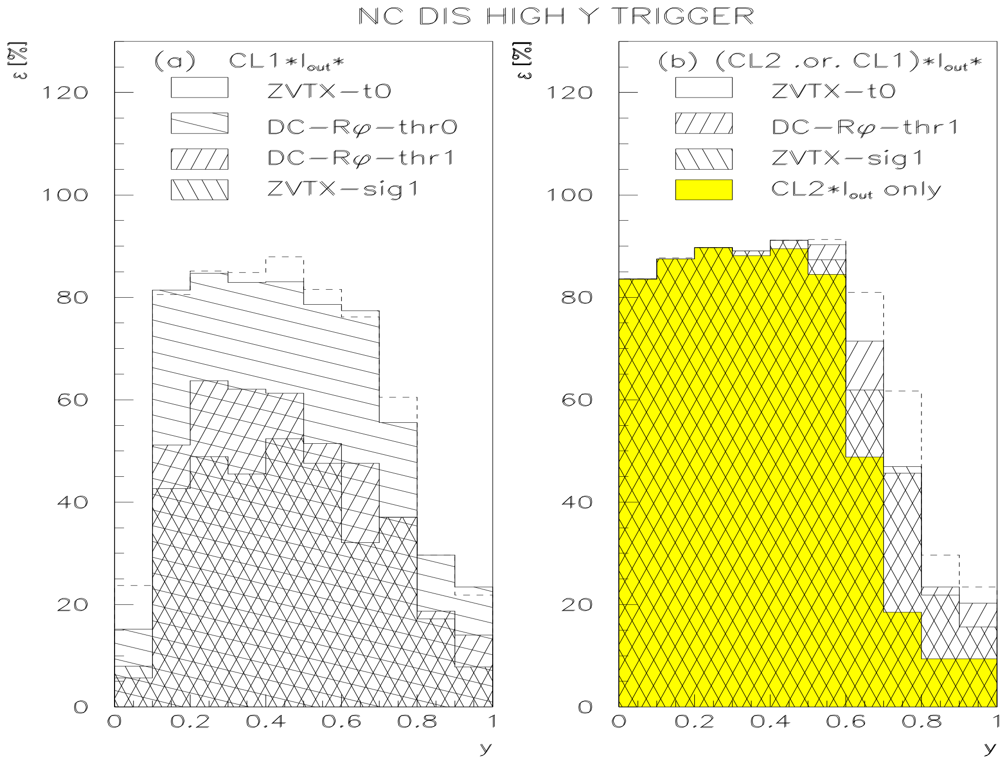

Figure 5.11: *The trigger y-dependence for $4\,GeV^2 < Q^2 < 100\,GeV^2$ with excluded innermost triangles from the cluster trigger. (a) $CL1 > 4.0\,GeV$ combined with tracker triggers. (b) It is seen that efficiency of $CL2 > 7\,GeV$ steeply falls down at $y > 0.6$ and that combined triggers are needed for the high y region.*

BSET in Coincidence with other Triggers

Common characteristics of all triggers put into coincidence with the BSET low threshold triggers in order to cover the high y region (Fig. 5.11) is that they are relying on correlations between a low energy electron in the BEMC and a hadronic activity in other parts of the H1 detector. Partons hadronization especially at low x is not very well known. It is a subject of extrapolations from higher x behaviour and therefore could be model dependent. As far as we don't have a reliable electron trigger at high y, the trigger efficiency cannot be measured directly from the data. Monte Carlo simulations are needed and model dependence must be studied. A short overview of the properties of the triggers proposed to cover the high y region in the kinematical plane is given here.

BSET$*$TOF-IA Here we use the fact that the BEMC is only an electromagnetic calorimeter, very transparent to hadrons which are mostly simply punching through the BEMC and TOF. So TOF-IA is most effective at $high - y$ and at $large - \theta_e$ (Fig. 5.12). Limited TOF angular acceptance ($\theta_e > 160°$) and possible dependence on the parton fragmentation assumptions complicate the final trigger acceptance (efficiency) calculation.

BSET$*$BPC Very high sensitivity to charged particles and its position in the backward region close to the beam pipe are reasons why BPC delivers high trigger rates. Major drawbacks are a not complete coverage of the BEMC and the lack of spatial information about hits on the trigger level. Requiring BPC coincidence with BSET cuts off the inner- and outer- most regions of BEMC (Fig. 5.12a). In order not to lose these events, these boundary BEMC regions should be predefined as always active for the BPC trigger. This needs some hardware changes in order to extract BSET information about activities in the outermost two columns resp. rows.

Nevertheless the BPC could be used, without any changes, as a veto against synchrotron radiation background if this turns out to be a serious problem.

BSET$*$ZVTX ZVTX trigger requires activity in the central and/or forward H1 region. It is not efficient to low y events, for which quasielastically backwards scattered electron and proton remnants in the very forward H1 region are typical characteristics.

BSET$*$DC-Rϕ The central drift chamber trigger angular acceptance is limited to $\theta \sim 25° - 155°$. Therefore its efficiency for $\theta_e > 155°$ is in fact only the reflection of hadronic activity in the central region.

BSET$*$FRW-t_0 Forward ray trigger covers the angular range $\theta \sim 7° - 25°$ and is sensitive up to rather low y. In order to explain the efficiency at low Q^2 the same arguments as for the previous trackers are valid.

BSET$*$(Trackers OR TOF-IA) $Tracks{-}t_0$, i.e. the 'OR' from all available tracker t_0 ensures coverage of the whole H1 angular range but at the same time is very sensitive to the background conditions. A better background rejection can be achieved by coincidence requirements as e.g. $ZVTX - sig1 * DC - R\phi - thr0$. On the other hand simultaneous decrease of physics efficiency is unavoidable. Reasonable compromise is determined by the background conditions.

To cover the central and backward parts the 'OR' between $ZVTX{-}sig1$ and $TOF{-}IA$ is very efficient. The background rates are in this case dominated by the $ZVTX$ trigger, the contribution of $TOF - IA$ should be negligible.

Trigger at Large Angles

Excluding the innermost triangles from the BSET cluster trigger allows to reduce the CL2 (at 6 GeV) rate almost by factor 20. The loss of events is ϕ dependent for $\theta_e \sim 173° - 175°$.

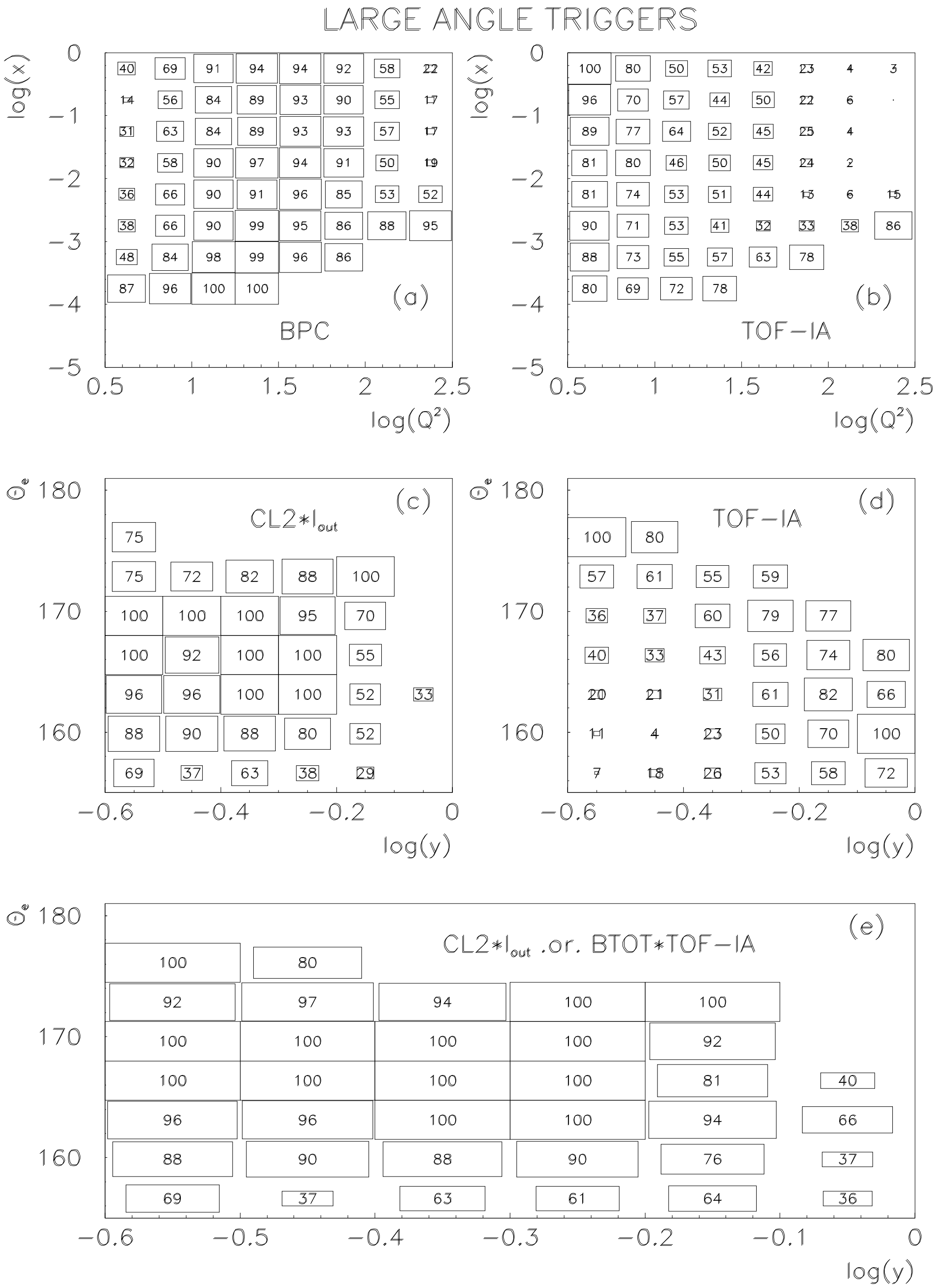

Figure 5.12: *(a), (b) BPC resp. TOF-IA trigger acceptance in log(x)-log(Q^2) plane. (c) $CL2$ trigger acceptance at large θ_e and high y with excluded innermost stacks. (d) Stand alone TOF-IA is complementary to $CL2*I_{out}$ (the same as (b) but now in $y-\theta_e$ plane). (e) Resulting acceptance if $CL2$ trigger is 'OR'ed with BEMC total energy put into coincidence with TOF-IA signal. Significant improvements at large angles and high y are observable when compared to (c).*

But this is no tragedy because the Q^2 of rejected events is below $10\,GeV^2$ and this is a region of bad acceptance where the systematic errors of the structure function F_2 measurements are above 10% (Fig. 1.3). So the real losses due to the exclusion of the innermost BEMC stacks from the trigger are negligible. Part of the physics could still be recovered by considering events with interaction points in the very forward region.

Scattering at low x and very large angles θ_e (in H1 coordinate system) or in other words with a very small deflection of incoming electrons reminds fixed target experiments. Hadrons from the current jet are in this case mostly produced into the backward region (Fig. 1.2). As already mentioned, parton fragmentation depends on the model assumptions and the central tracking detectors could or could not be sensitive to these kind of events.

A solution avoiding tracker triggers could be TOF-IA. TOF-IA is sensitive not only to punch-through hadrons but also to high energy electrons ($\sim 30\,GeV$) and close to the beam pipe to all electrons hitting only the BEMC edge. In order to profit from disabled triangular stacks HT (I_{out}) and still to be sensitive at large θ_e, the BTOT energy trigger could be used in coincidence with TOF-IA (Fig. 5.12e).

Despite all these problems the data with quasielastically scattered electron in the triangular stacks will be needed for their energy calibration. One solution could be to have dedicated runs for this purpose with the same or slightly higher HT as are used for all other stacks.

Another possibility is to set the innermost stacks HT at $10\,GeV$ (I_{10}) and to take data during all runs. For the CL3 trigger it would mean higher, but still acceptable background rate (Table 5.2). CL3 trigger can be even prescaled and for CL2, CL1 the veto from innermost stacks above HT ($\overline{IST}$) is equivalent to the exclusion of these stacks from the cluster trigger completely.

5.2.2 High Q^2 Events

As the results of the simulations show this region could be covered very well by any of the LAr triggers. Most powerfull is the e^--trigger. The energy depositions and rates from the beam-wall and beam-gas background in the barrel part of the LAr are small. Therefore the limiting factor for the lowest threshold here is the noise in the calorimeter read-out and trigger chain. The most difficult is the inner forward (IF) part of the calorimeter, where high rates with big energy deposits from the proton induced background are expected. Therefore the trigger threshold must be much higher than in other parts.

The most effective LAr triggers for the high Q^2 NC DIS found from the simulation studies are the following ones:

1. electron trigger (Fig. 5.13)
2. transversal energy - E_T
3. topological sums - E_{BAR}, (E_{FB}, E_{CB})

The LAr electron trigger [40] is based on two energy thresholds requiring some minimal energy in the electromagnetic part of the BT and allowing some maximal energy leakage into the corresponding hadronic part. This hadronic veto is supposed to reject hadrons which could fake electrons. Both these thresholds vary for the different parts of the LAr calorimeter (Table 5.4). They take into account the event kinematics and also the fact, that the electromagnetic calorimeter has not the same depth in all its parts (it changes from $20X_0$ in the central barrel to $30X_0$ in the forward barrel).

BT part	CALORIMETER PART		
	IF (inner forward)	FB (forward barrel)	CB (central barrel)
EM threshold (GeV)	30	10	8
HAD veto (GeV)	5	4	3

Table 5.4: *LAr second electron trigger thresholds in different parts of the calorimeter*

Therefore one has to set carefully the proper thresholds. E.g. a too low hadronic veto threshold could create holes in the trigger efficiency coverage of the $\log(x)$-$\log(Q^2)$ plane. However this could be compensated by the transversal energy E_T or e.g. barrel energy trigger. This is an illustration of the importance of trigger redundancy in the same kinematical region.

5.2.3 Subtriggers for NC DIS: Summary

From the trigger elements available at L1 level a lot of different combinations could be built. Some of them which have been simulated for NC DIS scattering are summarized below. Many of them are very similar in their acceptance and of course not all must be enabled simultaneously. With only a few of them the kinematical region of interest could be effectively covered. For example the achieved acceptance for the NC DIS with combination ('OR') of subtriggers 2, 6, 12, 16, 21 is shown on the Fig. 5.13.

1. $CL2 * \overline{TOF}$
2. $\mathbf{CL2} * \overline{\mathbf{IST}} * \overline{\mathbf{TOF}}$
3. $CL3 * \overline{TOF}$
4. $CL1 * ZVTX - t_0 * \overline{TOF}$
5. $CL1 * ZVTX - sig1 * \overline{TOF}$
6. $\boldsymbol{CL1 * DC - R\phi - thr0 * \overline{TOF}}$
7. $CL1 * BPC * \overline{TOF}$
8. $CL1 * TOF - IA * \overline{TOF}$
9. $CL1 * FWR - t_0 * \overline{TOF}$
10. $CL1 * Tracks - t_0 * \overline{TOF}$
11. $CL1 * ZVTX - sig1 * DC - R\phi - thr0 * \overline{TOF}$
12. $\boldsymbol{CL1 * \overline{IST} * DC - R\phi - thr0 * \overline{TOF}}$

13. $GE1 * ZVTX - sig1 * DC - R\phi - thr0 * \overline{TOF}$
14. $BTOT * ZVTX - sig1 * \overline{TOF}$
15. $BTOT * DC - R\phi - thr0 * \overline{TOF}$
16. $\boldsymbol{BTOT * TOF - IA * \overline{TOF}}$
17. $GE1 * ZVTX - sig1 * \overline{TOF}$
18. $GE1 * DC - R\phi - thr0 * \overline{TOF}$
19. $GE1 * TOF - IA * \overline{TOF}$
20. $ZVTX - sig1 * DC - R\phi - thr0 * \overline{TOF}$
21. $\boldsymbol{LAr - Electron * \overline{TOF}}$
22. $LAr - E_T * \overline{TOF}$
23. $LAr - E_{BAR} * \overline{TOF}$

A limiting factor for the central part of the LAr calorimeter trigger will be the noise in the trigger itself. The robust LAr triggers as electron, E_T or E_{BAR} topological sums will cover the high Q^2 region ($Q^2 > 100\,GeV$).

In the low Q^2 region the situation is more complicated. Background conditions are in this case dominating factors which determine the BSET energy thresholds.

Stand alone BSET cluster trigger could be used probably up to $y \sim 0.6$. For higher y values BSET energy triggers must be put into coincidence with trackers or TOF-IA triggers in order to cope with high background rates. Coincidence between tracker triggers only, as e.g. ZVTX*DC-Rϕ is also very useful for the problematic high y region. Tracker triggers are very efficient, a part from at low y, in the whole kinematical region but for these still more studies will be needed mainly on the possible model dependence.

A dedicated electron trigger at $large\,\theta - high\,y$ allowing to calculate trigger efficiency directly from the data as well as redundancy in the low Q^2 trigger is missing at present.

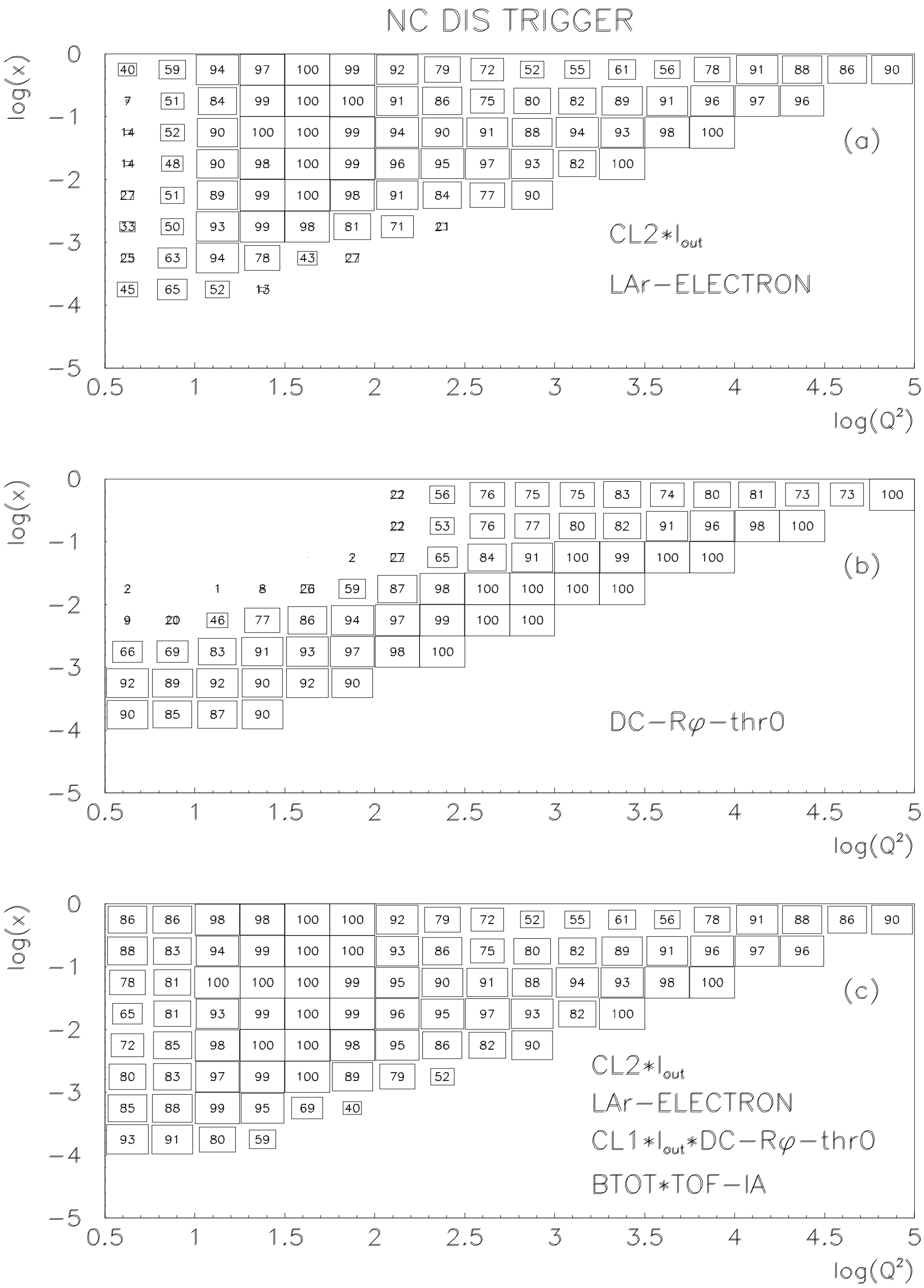

Figure 5.13: *(a) Trigger acceptance of LAr electron trigger and BSET CL2 with innermost ring excluded from the cluster trigger. (b) Acceptance of central drift chamber trigger. (c) L1 trigger acceptance for combination of 4 subtriggers only.*

Chapter 6

BSET Trigger - Hardware Realisation

6.1 Trigger Elements and Algorithm

The basic idea of the BSET trigger [53] is to look for well localized high energy depositions in the BEMC stacks. Groups of stacks with signals above preset thresholds are called clusters.

Cluster recognition is performed in a few steps. For this purpose the analog sums of EM channels from the same stack (*stack energy*) are used as primary trigger elements (*TE*) for the BSET trigger electronics. On the first level of pattern recognition the *cluster* is formed from up to 2×2 adjacent TE's (Fig. 6.1a). For each stack a set of 2 thresholds is defined. The programmable hardware of the BSET allows to require up to four conditions (C1-C4) to be fulfilled by the accepted event.

The BEMC subtrigger elements are then sent to the H1 central trigger logic, which can select any of these elements and combine them to form final H1 first level subtriggers.

C1: Number of clusters in the low threshold plane To recognize the number of clusters, the signals of the TE are compared in ATD modules (Amplitude and Time Discriminator) to the low threshold (LT). LT is set typically 2 - 3 σ above noise level. The resulting pattern of the output signals above LT (L_{th}) is then analyzed by the Cluster Identification Module (CIM) in three steps:

1. A search for a hit in the innermost 4 stacks is done. Each found hit together with the three adjacent stacks (if they have signal above threshold) is counted as one cluster. This information is recorded and the signals of those stacks are excluded from further analysis (Fig. 6.2).

2. The remaining pattern is analyzed using [X,Y] projections and memory look-up tables (LUT).

3. The resulting number of clusters is determined as a sum of those found in both previous steps.

The first step of the cluster counting can be disabled by jumpers on the CIM module and the second and third step are fully programmable. This means that the cluster size in the X and Y projections is not hardwired but can be redefined by the software and one can require some topological criteria, e.g. to have clusters back-to-back in the azimuthal angle ϕ.

C2: Number of clusters in the high threshold plane To recognize a candidate for an energy cluster, the stack energies are compared with the high thresholds (HT) in the ATD Modules. The stacks above HT, producing H_{th} signals, are the high energy cluster initiators ("seeds") (Fig. 6.1b,c,d). The resulting pattern of the H_{th} output signals is analyzed by the second CIM module the same way as in the case of low thresholds.

Both CIM modules are programmable to produce "KEEP" signals for 16 different cases e.g.:

- only one cluster is detected,
- at least one cluster is detected,
- at least two clusters are detected,
- more then two clusters are detected, etc.

C3: Cluster energy sums If at least 1 high energy cluster is found in the step C2, the cluster energy E_{cl} is determined.

If the stacks (TE) surrounding the "seed" (stack above HT) have signals above LT their energies are summed up (Fig. 6.1b,c,d). This sum is the cluster energy. Proper TE are selected by the Cluster Separation Module (CSM) and their signals are summed up in the Cluster Energy Modules (CEM).

In the case that more than 1 cluster was found one cannot assign to each cluster its energy and cluster energy is the energy sum of all clusters found (Fig. 6.1).

In the Energy Comparator and Timing Module (ECTM) three thresholds for cluster energies E_{cl} are implemented. These thresholds are used for independent down-scaling for different kinematic regions or in combinations with triggers from other subdetectors.

C4: BEMC total energy The total energy deposited in the BEMC E_{tot} is the sum of all stack energies above LT. The TE are summed in the CEM module and compared to the threshold level in the ECTM module. There is one threshold for the total energy deposited in the BEMC.

6.2 BSET Hardware

The BSET electronics is realized in 3 crates located in the H1 trailer. The analog electronics is located in 2 VME crates (VME mechanics and power supply distribution) and the digital electronics occupies one standard VME crate. The crates are located in the rack adjacent to the BEMC front-end electronics and are controlled by the dedicated BEMC OS-9 test station (TS) or by the main calorimeter processor. A schematic diagram of the BSET is shown in the (Fig. 6.3).

6.2.1 GAIN Card and ATD Module

Different stack types (quadrants, trapezoids and triangles) have different light collection properties. To achieve equal response from all stacks the signal weighting is needed. The trigger element analog signals from the stacks (88 TE) are equalized in the GAIN card and

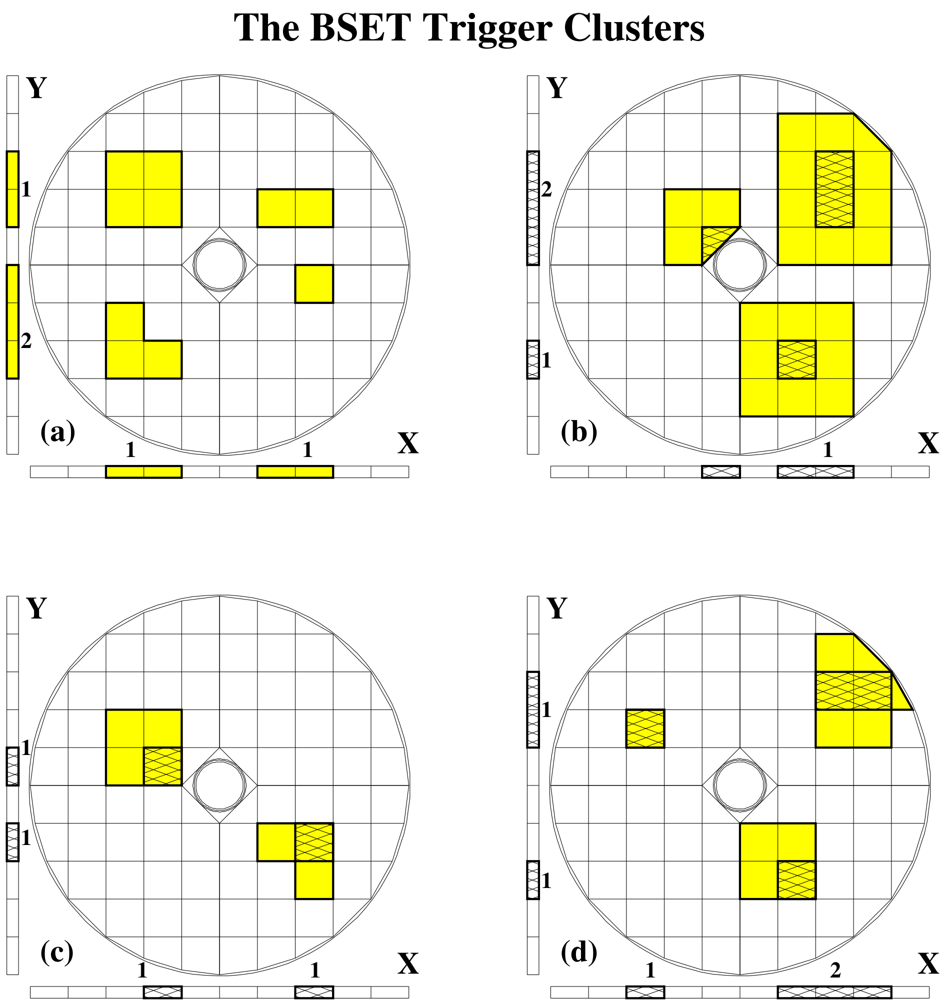

Figure 6.1: *(a) Examples of possible cluster configurations and their numbers as found in the (X,Y) projections. Limited precision of the clusters counting with this method is shown - only 3 out of 4 clusters are identified. (b) Cluster seeds (above HT - hatched) and all stacks which can contribute (shaded) to the cluster sum if they are above LT. (c), (d) Typical examples of the cluster form and size.*

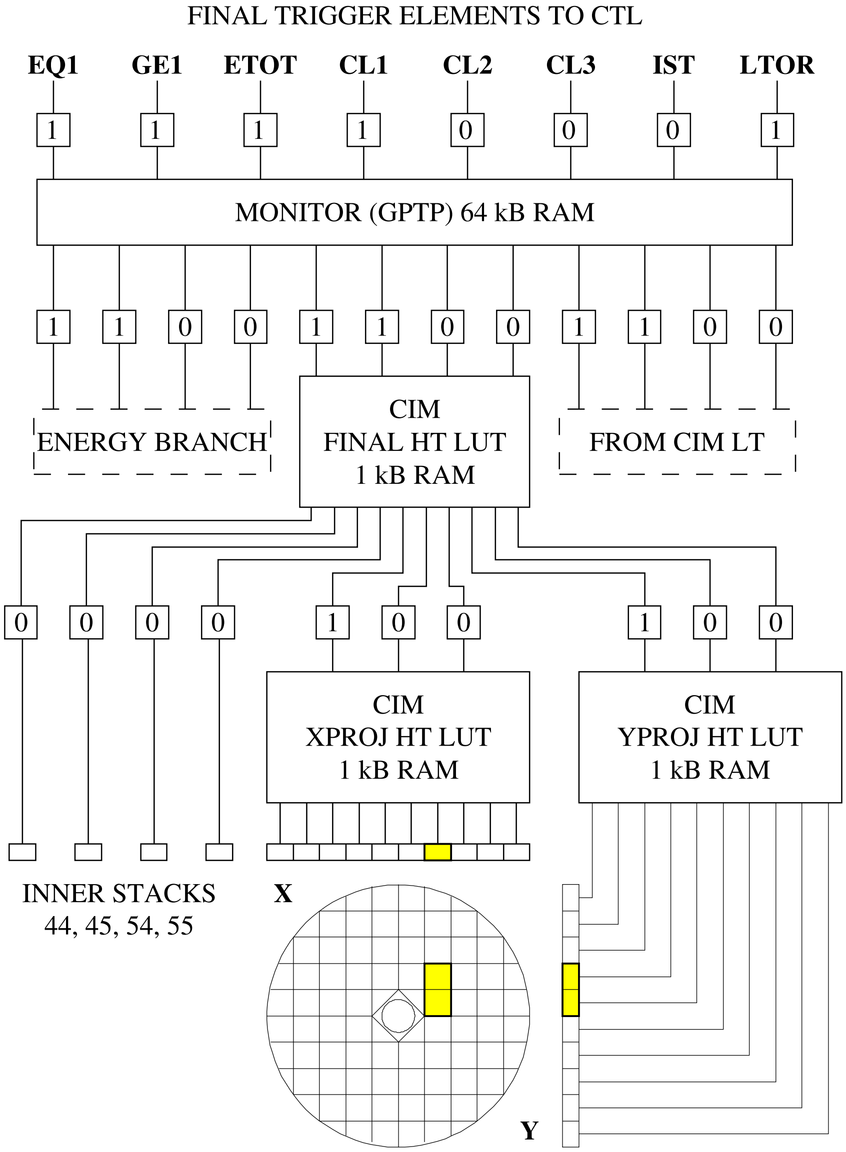

Figure 6.2: *Final BSET trigger elements production starting from the (X,Y) projections with following pattern recognition in the look-up tables (LUT). For simplicity reasons only high threshold (HT) path is shown - LT branch is completely analogical. In parallel analog energy branch produces energy sum bits (BTOT, CL1, CL2, CL3).*

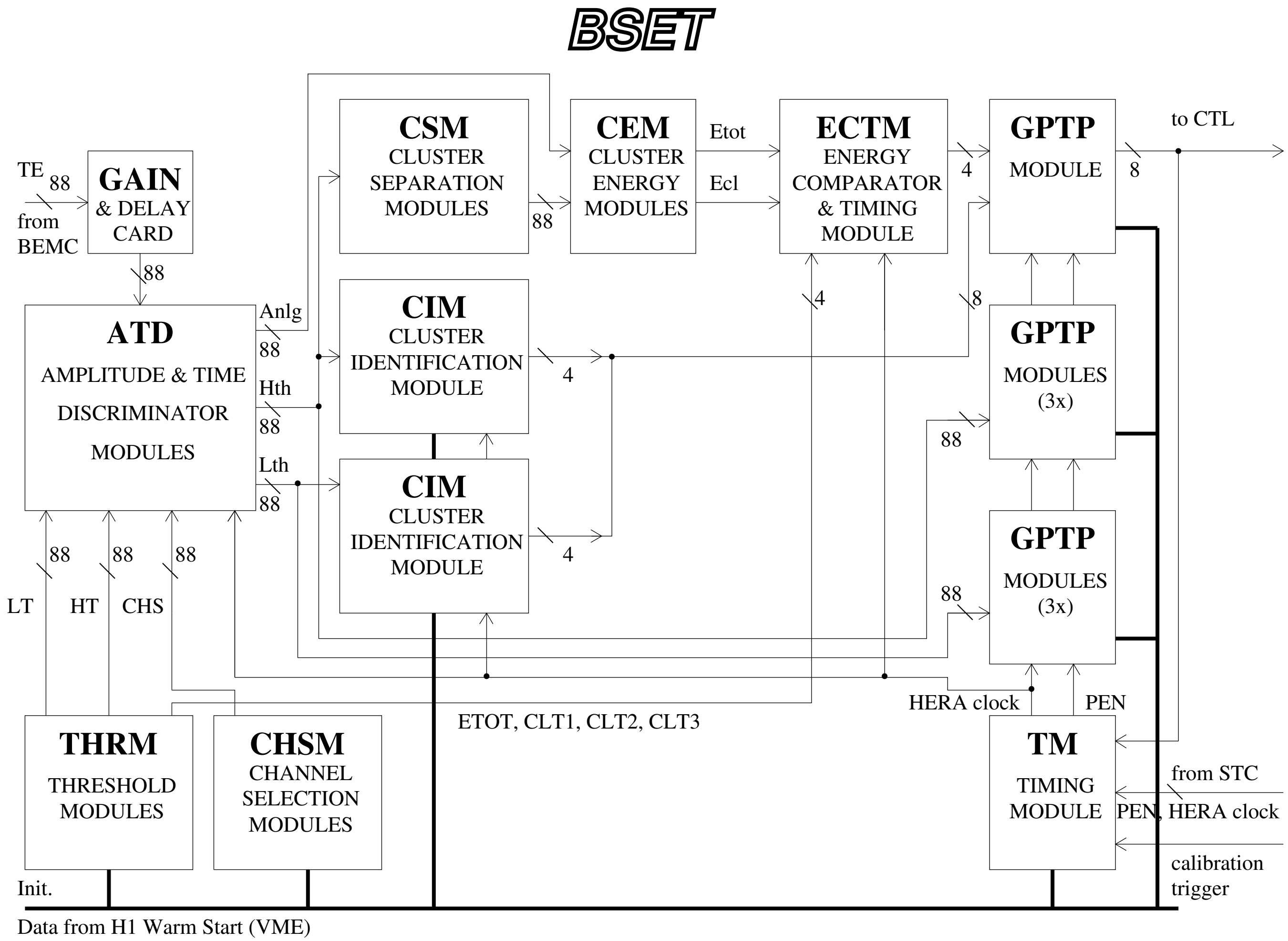

Figure 6.3: *BSET trigger block diagram*

are sent through mother boards to the analog Amplitude and Time Discriminator (ATD) module. The GAIN card contains also delay lines which allow time response equalization of all stacks.

There are 11 ATD-mother boards each with 8 ATD modules. The block diagram of the ATD module is in Fig. 6.4.

The stack energy signals are further processed in the ATD shaper. The ATD shaper is divided into three parts (Fig. 6.4).

The edge extractor sums the direct analog signal coming from the detector with the same inverted and delayed one. The delay of 120 ns ensures that the leading edge of the input signal is preserved on the output of this edge extractor. The falling edge of the output signal is 300 ns long.

This signal is afterwards differentiated and a bipolar pulse is created. Peak in the output signal from the edge extractor, corresponding to the t_0, is determined by the zero crossing detector.

The output signal of the differentiator is again integrated to get good energy resolution.

Finally, if a t_0 is detected, the output analog signal is gated with this t_0 for one bunch crossing period. The next HERA clock resets the t_0.

Each channel amplitude is compared to the 2 thresholds (LT and HT) and can be disabled for the case of hardware failures. Typical thresholds presently foreseen for the trigger operation are $LT = 0.8 - 1.3\ GeV$ and $HT = 3 - 15\ GeV$.

Short summary of the ATD module output signals:

1. L_{th}- digital signal, synchronized with HERA clock, indicating that the shaped analog signal from the stack is above low threshold (noise threshold). This signal is related to the peak position of the shaped signal (stack low threshold t_0).

2. H_{th} - digital signal with the same meaning as L_{th}, but for high threshold.

3. A_{nlg} - analog signal gated by L_{th} - input into the energy summing part.

6.2.2 CHSM and THRM Modules

The channel selection module (CHSM) gives a possibility to disable or enable the L_{th}, H_{th} and A_{nlg} signals simultaneously for each of 88 BEMC's stacks. This is done by setting appropriate bits in the 11 8-bit registers. An additional ($12th$) register is used to define 8 control signals for the Timing Module (TM) (see section 6.2.5).

The task of the 4 Threshold Modules (THRM) is to set 2 thresholds for each stack, 3 thresholds for cluster energy and 1 threshold for the total BEMC energy. Each THRM contains 48 8-bit DAC's for threshold setting. For threshold verification 48 ADC's are used.

6.2.3 CIM Module

The CIM (Cluster Identification Module) identifies energy clusters in the BEMC. The identification is done in both (L_{th}, H_{th}) BEMC threshold planes, i.e. in 2 CIM modules.

An energy cluster is defined as pattern of one or up to four (2×2) adjacent TE elements with signals over threshold (Fig. 6.1a).

The implementation of the cluster identification algorithm in the CIM module is shown on the Fig. 6.2.

The cluster recognition itself is based on the projections onto 2 orthogonal axes [X,Y]. This means that the search for stacks with $H_{th}(L_{th})$ signals is done in rows and columns. If at least 1 such stack in the row (column) is found the proper projection bit is set. Each of the [X,Y] projection patterns is written into the corresponding 10 bits (Fig. 6.2).
The resulting projected pattern is evaluated by the programmable look-up tables. In these tables parameters as e.g.: cluster size, number of clusters and topological criteria are encoded.

The output from these tables is coded into 3 bits for each projection.

The innermost 4 stacks are treated separately (see 3.C1) and the corresponding bits together with 2×3 bits from [X,Y] analysis are sent into the next LUT. Here this 10 bit information is summarized and the final result - 4 bits from one CIM module entering the monitor LUT are produced.

6.2.4 CSM, CEM and ECTM Modules

The CSM (Cluster Separation Module) produces digital signals enabling a contribution of analog A_{nlg} stack signals to the cluster sum. The CEM (Cluster Energy Module) is a summing amplifier, which produces the particular sum for the total BEMC energy E_{tot} and the particular sum for cluster energy sums E_{cl}.

The ECTM (Energy Comparator and Timing Module) switches trigger bits on if the energies fulfil the corresponding threshold conditions. On the output the following 4 trigger bits are produced:

- 1 bit for the total energy deposit in BEMC E_{tot}
- 3 bits for the cluster energies E_{cl1}, E_{cl2}, E_{cl3}

The layouts of modules CSM, CEM and ECTM are shown on (Fig. 6.4).

6.2.5 TM Module

The timing module (TM) is working as an interface for control signals between the BSET trigger electronics and the H1 central trigger logic (CTL). The TM module receives L1/L2 trigger control signals and HERA clock from the BEMC STC (Subsystem Trigger Controller) [54] fanout module and distributes them to the BSET hardware. It sets the appropriate delay for the HERA master clock, sets additional overrun delays and generates the local trigger signal. The following signals are used by the TM module to control different modes of BSET operation:

1. local or central mode
2. pipeline enable
3. trigger enable

4. random trigger

5. calibration trigger

6. - 8. after run (overrun) bits

For more details see section 6.3.

6.2.6 Monitor (GPTP) Modules

The output patterns of ATD modules (2×88 bits - L_{th} resp. H_{th}), the trigger conditions C1-C4 and the BSET subtrigger elements are stored for every bunch crossing in the General Purpose Trigger Pipe (GPTP) cards designed in the H1 collaboration [55]. These cards provide storage for 32 bunch crossings (BC). The BSET history information is very useful for pile-up detection mainly in the BEMC readout chain but also for other subdetectors. It is also used for timing adjustment, t_0 detection study, stability and integrity checking as well as calibration of the trigger electronics in the pipelined environment. This information is read out by H1 calorimeter readout branch and is available in the BSET BOS bank (all 32 BC or only 5 BC are read in the so-called extended resp. compact readout mode).

The resulting 8 BEMC subtrigger bits are provided for every bunch crossing (Δt= 96ns) via a programmable 64 Kbyte monitor look up table.

6.2.7 BSET Timing Characteristics

For proper synchronization of the BSET with the HERA clock and with other L1 triggers the knowledge of the BSET internal timing properties is needed.

An internal BSET decision time of 6 bunch crossings originates from the ATD and the CIM modules. The ATD modules need 3 BC to deliver the signals to the following CIM resp. CSM and CEM modules (see Fig. 6.3). The CIM decision is taken in another 3 BC. The parallel energy branch (CSM, CEM and ECTM) is faster and produces output signals after 1 BC already. To synchronize these two branches on the input into the GPTP card the selectable delay switch in this card is set to 2 BC to delay the ECTM output bits.

The internal delay of the GPTP card adds another 2 BC [55] resulting in the total BSET decision time of 8 BC. To be more precise the analog delays used to adjust the timing of the different stacks in the GAIN card (few tens of ns) should be added to the total decision time.

In the CTL logics the BSET trigger information is delayed by another 9 BC in order to be synchronized with all other triggers. This delay is determined by the slowest H1 trigger element entering the CTL (LAr trigger after 2.1 μs).

6.3 BSET Operation Modes

The BEMC electronics (readout and trigger) is an integral part of the H1 calorimeter readout branch. In such a large and complex system as H1 there is a need to have the possibility to test and tune the subsystem electronics independently. The BSET hardware is therefore designed to operate in three different modes :

1. Stand alone test mode

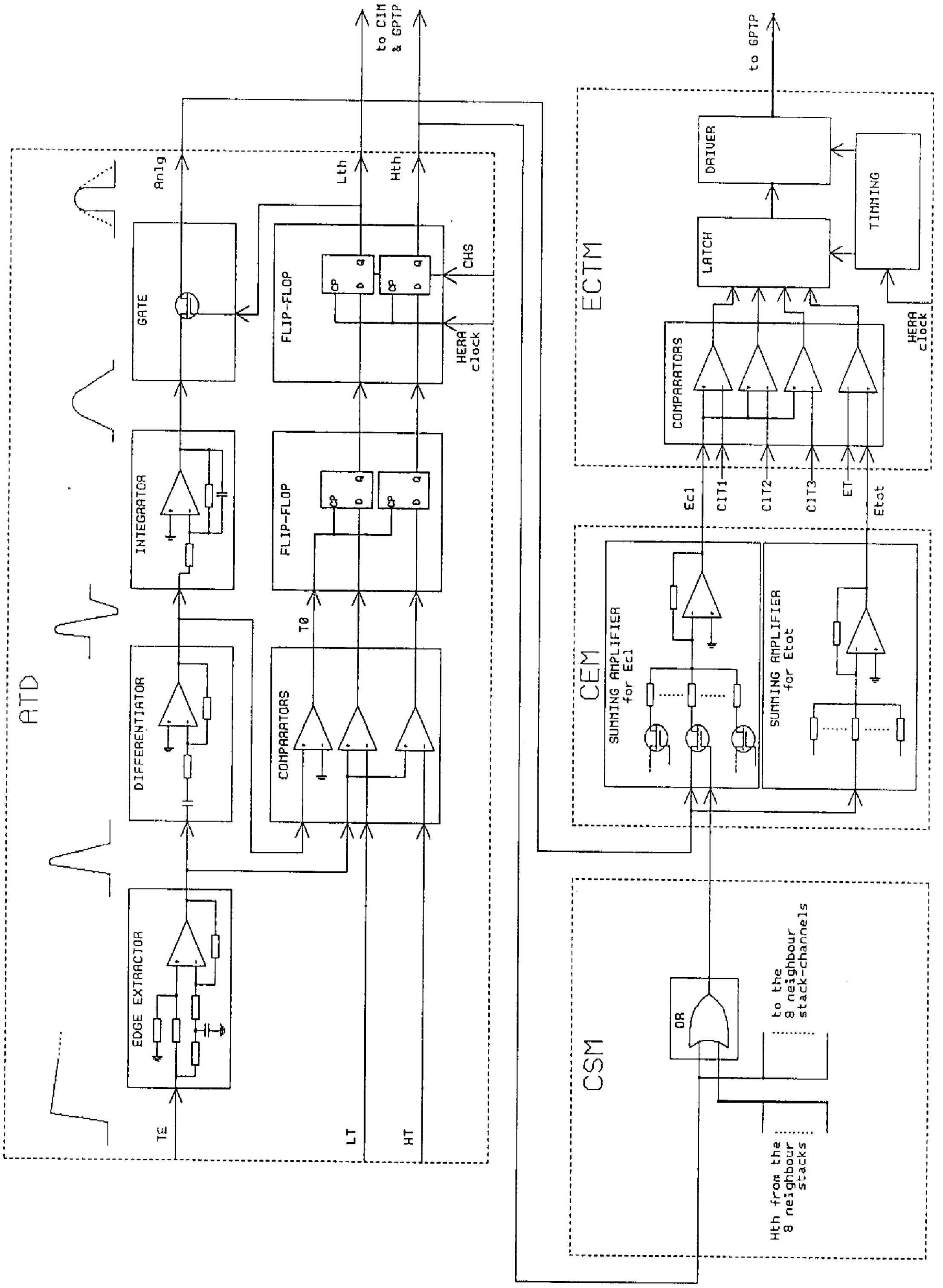

Figure 6.4: *Block diagram of the ATD module*

2. Stand alone e^-p mode
3. Standard data taking mode (central mode)

Stand alone test mode This mode allows to test, debug, tune and calibrate the BSET hardware completely independently. The BEMC test station sets up this mode (in TM module), chooses local trigger type and pulses the BEMC stacks with the BEMC calibration pulser [42].

The BSET provides three types of local triggers which are used for consistency checks of the whole trigger logic. They are called : *random, calibration* and *stand alone trigger.*

A *random trigger* is produced by the software of the control computer which stops the pipeline randomly. This trigger is used for pedestal and noise studies.

A *calibration trigger* is produced by the BEMC calibration pulser when the selected BEMC stacks are pulsed by a given DAC pulse height value. The calibration trigger is used for the gain, timing and threshold calibration of the trigger channels.

A *stand alone trigger* is one of the resulting 8 BSET subtrigger elements monitored locally. This bit is in the stand alone e^-p mode used as one of the local triggers. As the final subtrigger elements are produced via the fully programmable lookup tables, the stand alone trigger is used to test integrity and functionality of the whole BSET.

An activated local BSET trigger initiates the BEMC test station to read simultaneously data from the BEMC readout chain and from the trigger branch stored in the GPTP cards. Having both, trigger and readout chain data, together with three types of triggers provides powerful tools for testing, debugging and calibration of the trigger electronics.

Stand alone e^-p mode In this mode real data from the BEMC readout and BSET trigger are taken by the local BEMC test station using the stand alone BSET trigger or any trigger coming from the STC (H1 L1 trigger). The stand alone e^-p mode allows efficient tests of the BSET trigger response on real events.
Combining data from ADC and BSET chains allows optimal timing adjustment and thresholds calibration with real e^-p events.

Standard data taking mode In the standard data taking mode the local BEMC test station is not used and both branches (BSET and BEMC) of the readout electronics are controlled by the main calorimeter processor. In this mode the BSET trigger is regarded by the H1 central trigger logic as a standard triggering device. The BSET sends subtrigger elements to the CTL and through the STC receives H1 control signals.

6.4 Calibration and Timing Adjustment

6.4.1 Electronic Calibration of the Trigger

The goal of the calibration procedure is to find a function that converts the threshold settings to actual energy values in the corresponding BEMC stack. Energy in the BEMC stack is represented by the DAC pulse value of the calibration generator. To get one point of this function the following procedure is applied. For a given threshold (LT or HT) the stack is pulsed with different DAC levels in the region, where the transition in the efficiency curve is expected. For each DAC value a given number of pulses is generated and the efficiency is then represented by the fraction of events for which the signal above threshold (in the right time slice) was detected. Differentiation of the efficiency curve gives a peak position at the threshold value.

The points obtained from this procedure are fitted by a linear function and the fit parameters $p_1(gain)$ and $p_2(pedestal)$ are plotted versus channel number. The same calibration procedure is done for low and high thresholds. The final results are used for thresholds setting of different classes of physics events to be triggered.

6.4.2 Timing Adjustment Procedure

In the collider type (pipeline mode) of the trigger electronics there are two basic timing related problems:

- adjusting of all subtrigger elements from the specific detector to the same bunch crossing
- setting the optimal delay for the main accelerator clock and the clock used in the trigger electronics

Thus the timing adjustment procedure has two major steps.
In *the first step* the calibration generator is used to find the BSET channel timing spread and the individual delay for each of BSET channel is determined. From the t_0 distribution for one BSET channel we can see that some of the t_0 values are found in the wrong BC. For each channel the efficiency of signal detection in the right BC for different time delays is computed. Scanning in 5 ns steps in the range of 2-3 BC's around the assumed t_0 position provides the optimal time delay at which the full efficiency is achieved. This procedure can be done individually for each channel or for all channels simultaneously. The distribution width of measured delays must fit into the 1 BC time interval.

The task of *the second step* of the timing adjustment procedure is to find the optimal delay between the HERA clock (from the STC) synchronizing the BSET hardware and the BSET trigger bits position inside the right BC found in the previous step. Here one must take into account the energy dependence of the signal's timing position. This is very important in order to cover the whole dynamic range of the real physics signals.

Chapter 7

BSET Trigger Performance

7.1 Introduction

The trigger efficiency for a given physics process is the goal of each trigger performance study. But before obtaining the final number a lot of technical checks connected with the whole data acquisition process has to be done. Therefore we divided our analysis into two steps:

- **trigger technical performance**
  - Performance of the individual stacks which are the basic trigger elements - most important is timing of each individual channel (see previous Chapter, page 82). We must ensure that for the whole dynamic range the stack response will be always in the same BC. Noise levels should be known and the low thresholds (LT) should be set to $3 - 4\ \sigma$ above the noise (noise thresholds).
  - verification of the encoded logic
  - verification of the summing part
- **trigger physics efficiency**
  - threshold determination in a GeV energy units for all trigger elements
  - efficiency calculation for certain class of physics events

Almost all these checks are in principle based on the *comparison* of the *reconstructed energy* from the analog read-out chain with the *trigger response* to these signals.

Another possibility is to find some *independent physics triggers* suitable for *crosschecking* the performance of our triggers. In our case the tracker triggers as e.g. BPC, ZVTX, TOF or DC-$r\phi$, are used.

In the experiment a set of the so-called *monitor triggers* is defined, used to monitor the performance of the corresponding *physics triggers* and supposed to represent a very small fraction of the all collected data.

7.1.1 Trigger - Reconstructed Energy Correlations

Before calculating the BSET efficiency, we want to stress that we distinguish two classes of energies, when talking about the trigger efficiencies:

1. **trigger energy** - energy seen by the BSET trigger;
   - *trigger cluster energy* - i.e. energy sum from the stacks above the low threshold adjacent to the stack above high threshold (trigger cluster initiator)

- *trigger total energy* - energy sum from all BEMC stacks, which are above low thresholds

2. **reconstructed energy** - energy from off-line reconstruction
   - *leading cluster* - cluster with maximal energy from all reconstructed clusters
   - *total cluster, total energy* - sum of all reconstructed clusters [56], equivalent to the total reconstructed energy

The fact that the clustering algorithms are slightly different in the trigger and in the reconstruction, that a trigger cluster requires at least one stack above high threshold ($\sim 3\ GeV$) and to the trigger cluster sum contribute only stacks above low threshold ($\sim 1.3\ GeV$), the trigger and reconstructed cluster energies could be significantly different (Fig. 7.1). Also total energies from reconstruction and seen by the trigger are different due to the low threshold condition for trigger total energy.

7.1.2 Thresholds and Efficiency Functions Evaluation

The calibrated thresholds and the trigger efficiency as a function of the deposited energy are obtained from the following general procedure:

- the reconstructed energy for the given channel (stack) or variable (cluster, total energy) is accumulated with sufficiently high event statistics into two histograms; into the first one enters all events and into the second one only those triggered by the studied trigger
- the trigger efficiency as a function of energy is obtained by dividing these histograms
- the resulting histogram is fitted with the modified 3-parameter Fermi-Dirac distribution function:

$$\epsilon(E_i) = \frac{P_3}{\exp\frac{P_1 - E_i}{P_2} + 1}[\%] \tag{7.1}$$

Parameter P_1 is the threshold value, defined as the energy at which trigger efficiency reaches 50%. Parameter P_2 describes the width of the transition region (threshold width) and at $\pm 3 \cdot P_2$ the efficiency reaches 95 % resp. 5 %. The third parameter P_3 fits the maximal achieved efficiency.

In the trigger efficiency histogram three regions, with different efficiencies can be distinguished:

1. *inefficient region* - energy is far below the set threshold
2. *threshold region* - energy is around the threshold and efficiency is rising from zero to its maximal value
3. *efficiency plateau* - efficiency is almost constant and for good triggers very close to 100%

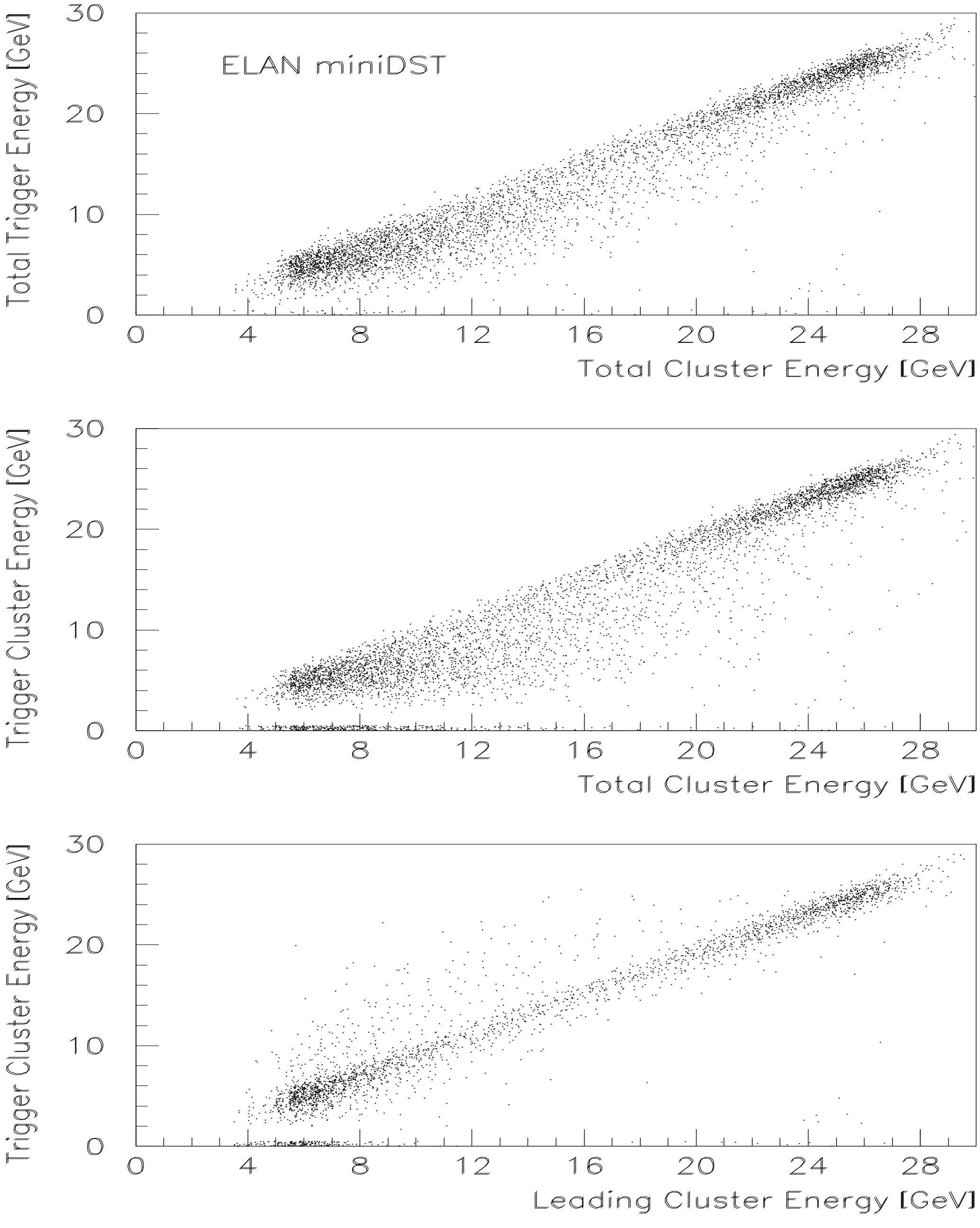

Figure 7.1: *Correlations between energies seen by the trigger and from the reconstruction.*

7.2 Technical Performance

7.2.1 On-line Monitoring of the BSET Triggers

Each trigger has to be checked already on-line, during the data taking, in order to detect problems as soon as possible. Any inconsistencies in the trigger logic, dead and/or noisy channels could deteriorate the quality of the measured data. Off-line corrections at the physics analysis level are very often painful and difficult. The time and informations available for on-line monitor task are usually rather limited, but nevertheless monitoring significantly improves the measured data quality.

Monitoring can be done on each of the H1 trigger levels L1-L4. As already mentioned, in the first period of the data taking only levels L1 and L4 were used. The most elaborated on-line monitoring of the BSET trigger was done on the μVAX cluster by requesting events from the event builder (AMD29000 RISC processor) [57] via the calorimeter OS9 station. The available information, i.e. the time history of all BSET trigger elements and uncalibrated energies from each BEMC readout channel (diodes), was provided by the calorimetric Digital Signal Processor (DSP). At that time the information from the Central Trigger Logic (CTL) was not available on this stage. The missing L1 trigger results, i.e. the information which subtrigger initiated L1-keep complicates unambiguous identification of the potential problems. E.g. if some other trigger had timing problems and was activated earlier, at first glance this can be identified as some "malfunctioning" of our monitored trigger. But a more detailed analysis could reveal that the expected trigger bit is active 1 bunch crossing later, i.e. monitored trigger works correctly and the shift is due to other trigger which is out of the time. From the many of histograms written to monitor the BSET performance on the μVAX cluster the following ones proved to be the most usefull:

- hit maps for each trigger element - this kind of histograms helped to identify 2 sorts of hardware problems: noisy and dead channels.

  Noisy stacks were identified in the 2-dimensional scatter plot with stack number on the x-axis and the bunch crossing (BC) position on the y-axis. On the Fig. 7.2/53 is an example where the LT trigger bit of the stack 56 is very noisy and is always active. This fact is reflected also in the behaviour of the trigger elements using this information, namely in the number of low energy clusters (Fig. 7.2/55). The quiet behaviour of stack high thresholds is shown on the Fig. 7.2/54. HTs are without the noise signals outside the nominal BC position.

  Identification of dead channels was done by selecting stacks with energy deposit (from DAQ branch) safely above the HT and checking if also the corresponding stack threshold trigger bit has fired.

- cluster and total energy thresholds

- stack energy thresholds (LT, HT)

- relative rates of different trigger elements - they served mainly as a logic consistency check, e.g. comparison of rates from three cluster thresholds $CL1 < CL2 < CL3$ (Fig. 7.2/5), or the ocurrence of trigger elements EQ1 (1 high energy cluster) or GE1 (at least 1 high energy cluster found)

- number of hit stacks above LT and/or HT thresholds (Fig. 7.2/6,7)

7.2.2 Stack Performance Check

The basic ingredient of each BSET trigger element is the BEMC stack. Therefore we have to know and understand the performance of each stack. When studying the occurence of low and high threshold (LT, HT) bits of individual stacks two types of inefficiency can be identified:

- LT(HT) bit is not set in the proper bunch crossing (BC) but in another one
  - this can be a sign of pileup, i.e. there can be a real signal at a different time, in another BC
  - this can be also timing problem of the trigger; when individual channels are not precisely adjusted in time, then too small or big signals can cause a shift towards the previous, resp. next BC
  - this can be a general trigger timing problem; if an event is triggered by a trigger which is not stable, then we can derive this "missing" information from our trigger
- the LT(HT) is not set in any of the recorded BC's, although the energy deposit is highly above the threshold
  - this is the case of hardware failure, reflected in the real stack trigger inefficiency and projected of course into the energy sums (total and cluster).

7.2.3 Logic Consistency Check

The logic consistency check in our case means testing the correctness of the trigger results and looking for events in which the active bits are in some logical contradiction. E.g. the rate of the trigger element $GE1$ cannot be lower than that of $EQ1$.

Checks of the logic consistency are done already during on-line monitoring and in more detailed analysis off-line, where the status of the trigger bits is compared with the off-line reproduced trigger information. This is done by applying the same trigger algorithms, as are supposed to be loaded in the look-up tables, on the reconstructed energy deposits in the individual stacks. Very helpful, at revealing errors in the look-up tables, especially in the first phases of the data taking was the graphical software package H1ED - event display [58]. This tool enables a very detailed event scanning by eye, and confronts the trigger information with the energy deposits in the individual stacks.

7.2.4 Verification of the Summing Part

Verification of the performance of the CSM (Cluster Separation Module), CEM (Cluster Energy Module), and of the ECTM (Energy Comparator and Timing Module) is in principle done in the following steps:

- the fired HT and LT bits of the individual stacks in the nominal BC number are found

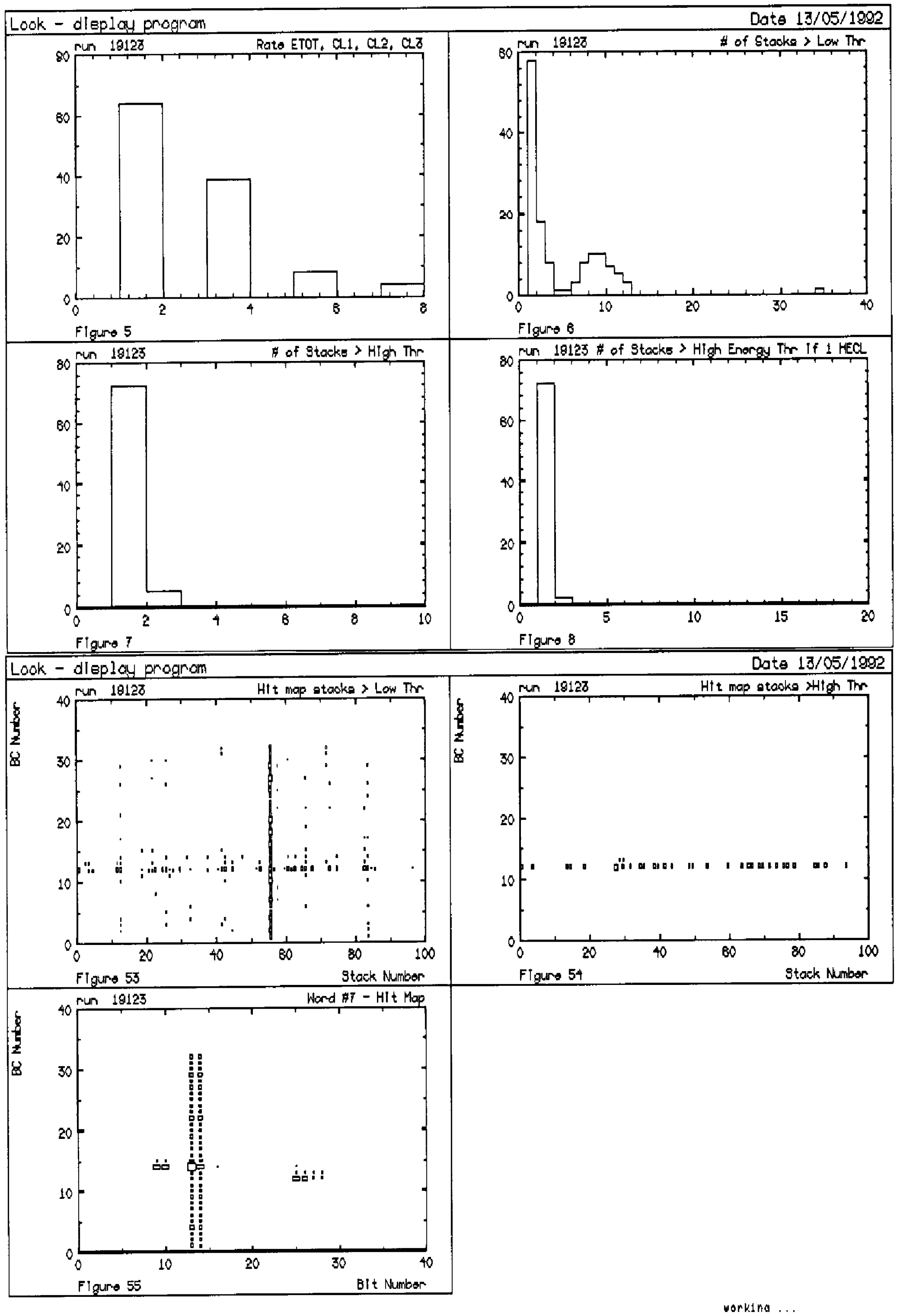

Figure 7.2: *Examples of some on-line histograms monitoring the BSET trigger performance on the μVAX cluster.*

- the energy from the data aquisition part for these stacks is taken and with the same algorithm as in the trigger logic the BEMC trigger total and cluster energy sums are created
- the response of the cluster (CL1, CL2, CL3) and of the total energy (BTOT) bits is checked
- the efficiency for these bits is calculated

Examples of efficiency curves for all our trigger energy sums from one period of the data taking, obtained by this verification procedure, are shown in Fig. 7.3. A characteristic feature of these curves is the narrow transition region, steep efficiency rise and 100% efficiency on the plateau above some threshold. The width of the threshold region depends on the relative precision of the individual stacks calibration, on the precision of each stack thresholds setting and finally on the number of stacks contributing to the trigger energy sum. The main physics trigger CL2 shows the typical behaviour as mentioned above. In the case of CL3 insufficient statistics prevents detailed studies. For CL1 the effect of events selection cut, requiring at least 2 GeV energy cluster in BEMC, is seen.

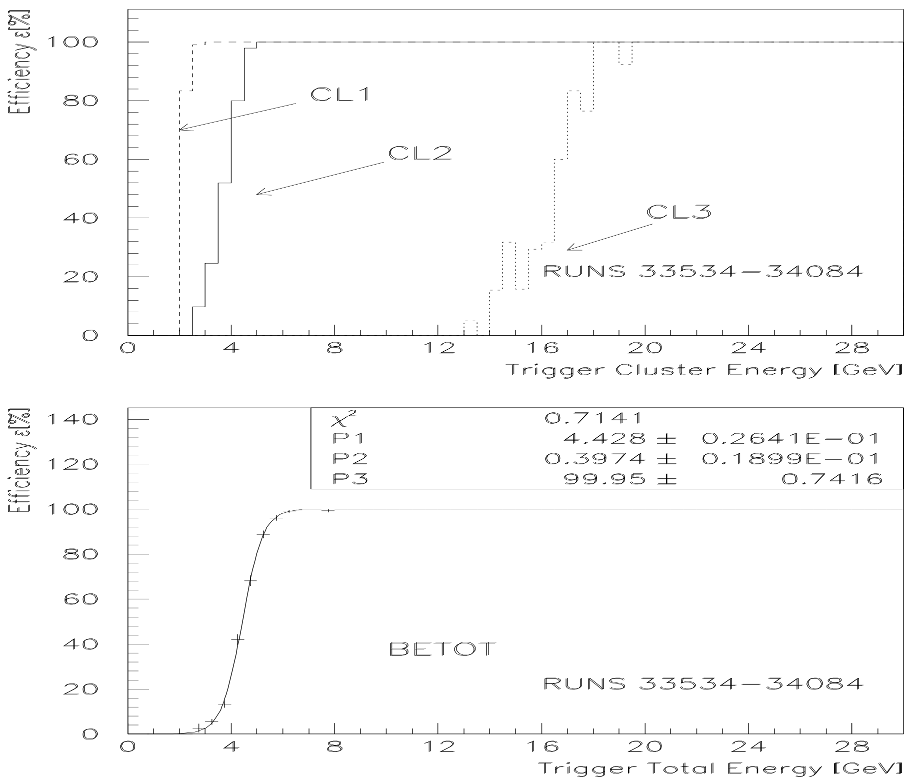

Figure 7.3: *Trigger efficiencies for cluster energies seen by the trigger (a) and total BEMC trigger energy fitted with Fermi-Dirac function (b) 7.1.*

7.3 Physics Trigger Efficiency

7.3.1 Stack Thresholds

Each stack is compared with two threshold levels as discussed earlier. The stack thresholds are independent of each other and different thresholds can be set for each stack. So e.g., for the stacks closest to the beam pipe higher thresholds should be set, compared to those located further from the beam line. This is one of the tools for handling high background rates, but of course it complicates final acceptance calculation.

Low Thresholds (LT) Low thresholds setting takes into account different noise levels of individual stacks and LTs are intentionally not the same. The differences between different stacks are seen from Fig. 7.5. The mean value over all stacks is 1.3 GeV (Fig. 7.6). The entries into this histograms were obtained for each individual stack from the standard efficiency calculation procedure (sec.7.1.2). The same result is obtained by application of the standard procedure on the sum of all stacks.

Extreme values at $LT < 1.0\ GeV$ belong to the small triangles. They show better noise behaviour (only 3 diodes), therefore could be set so low. The LT were not changed during the whole autumn 1992 data taking period.

High Thresholds (HT) The HTs for all stacks were set to the equal DAC (Digital Analog Converter) values. The only exception were the innermost triangular stacks. Their HT were set to the maximal value of 255 DAC units ($> 100\ GeV$), and this way they were excluded from the trigger as a potential cluster initiators.

Gradually as the performance of the HERA machine was improved and the background rates decreased, the HTs and energy sum thresholds were lowered. Four different HT settings are available and we can calibrate our stack trigger threshold values, given in DAC units, directly from the data. Thresholds for all stacks together are shown in the Fig. 7.4. Rather broad threshold regions indicate, that there are differences between individual stacks. The same DAC value does not ensure the same energy value. In the measured region we have observed a very good linearity and the calibration curve for the mean thresholds (average over all stacks) is fitted with a linear function:

$$HT(GeV) = (0.024 \pm 0.129) + (0.456 \pm 0.019) \times DAC \tag{7.2}$$

7.3.2 Total Energy Thresholds

To the total energy ($BTOT$) trigger element contribute all stacks with energies above LT. On the off-line reconstruction level a total BEMC energy is obtained from the sum of all reconstructed clusters and for this variable $BTOT$ physics thresholds are estimated. During the 1992 period BSET total energy trigger was running at three different DAC values (10,15,24), what in terms of the total reconstructed energy means 2.4 ± 0.3, 3.9 ± 0.3, $5.7 \pm 0.4\,GeV$ respectively.

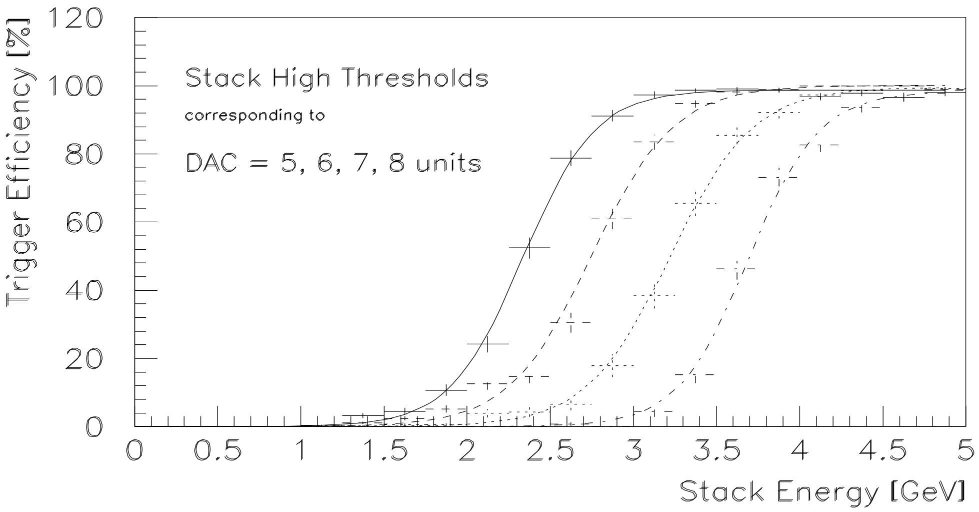

Figure 7.4: *Stack high thresholds corresponding to different DAC values*

7.3.3 Cluster Energy Thresholds

Cluster trigger thresholds (CL1, CL2, CL3) were changed more often, but not all values are usable for the calibration. Sometimes insufficient statistics is the reason, but mostly cluster threshold (mainly CL1) was very close to the HT (even below) and de facto determined by the stack high threshold. CL2 was used as a main physics NC DIS trigger, whereas CL3 was set as a kinematical peak trigger and monitor for the TOF performance. In principle seven different points, seven different DAC values are available for the cluster thresholds calibration. The *GeV - DAC* dependance was fitted with the function:

$$CLT(GeV) = (-1.68 \pm 0.04) + (0.36 \pm 0.003) \times DAC \tag{7.3}$$

7.3.4 Efficiency for the Low Q^2 NC DIS

When estimating trigger efficiency for certain class of physics events the first question we ask is:

- Does the trigger quantity correspond unambigously to the physics variable (object) we rely in the analysis on?

In the case of affirmative answer on the first question, the trigger efficiency calculation can be relatively simple. In principle the trigger efficiency then depends on one variable. In the other case, the task starts to be more complicated and we have to take into account all specifications of the trigger definition and of the physics analysis. The trigger efficiency depends on more variables, which are correlated and its calculation then becomes a multi-dimensional task.

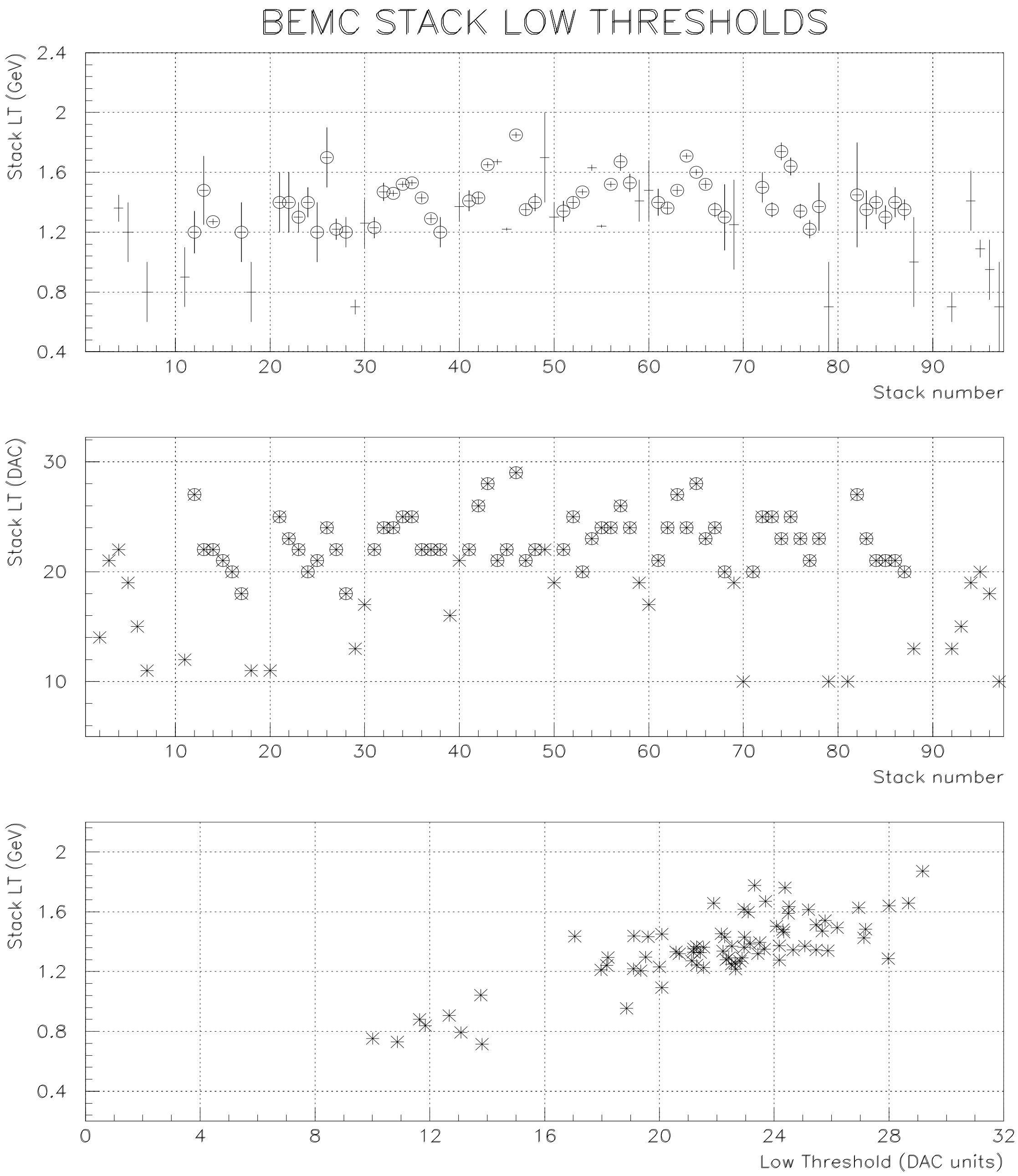

Figure 7.5: *Stack low thresholds in GeV (a), in DAC units (b) and correlation between them (c). In (a), (b) the circles stand for the quadratic stacks, the rest are trapezoids and triangles.*

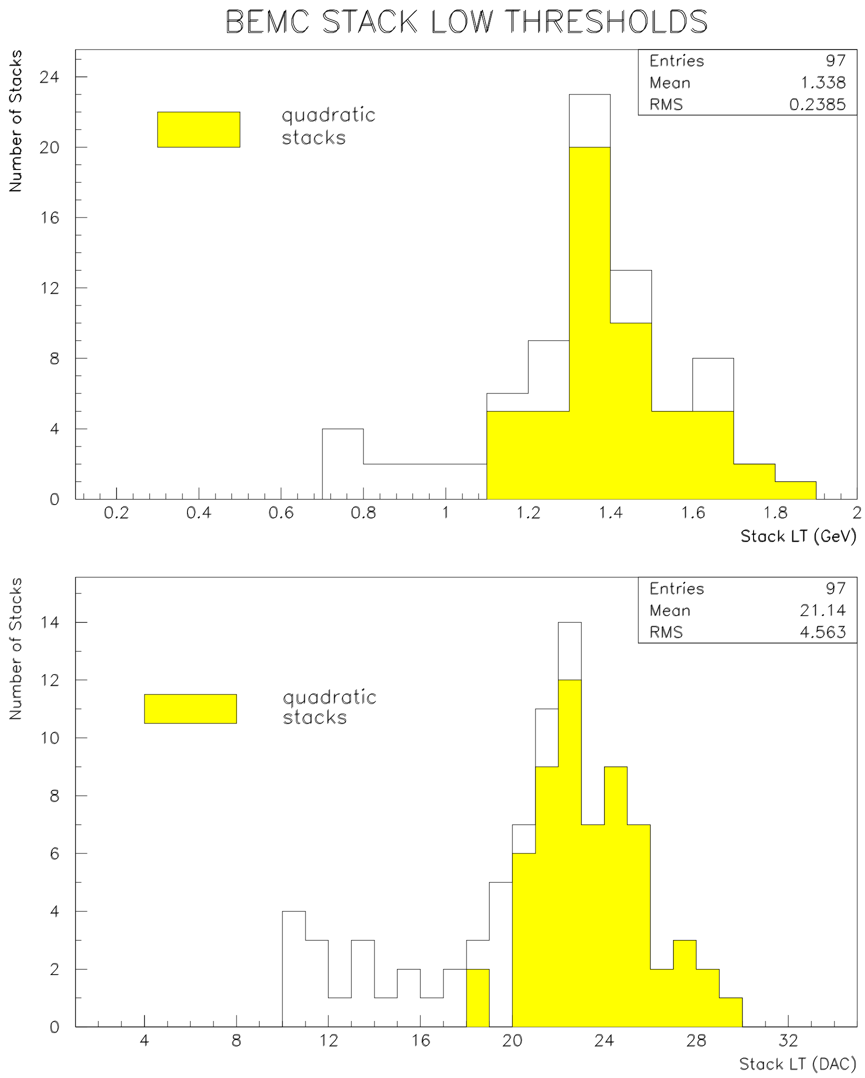

Figure 7.6: *Stack low thresholds distribution for all stacks in GeV (a), and in DAC units (b).*

It is important to note that the BSET trigger is not a truly inclusive electron trigger since in the case when more trigger clusters are found, the resulting trigger cluster energy is the total energy sum of all these clusters.

Therefore the determination of the trigger efficiency must be done on the total energy sum of all reconstructed clusters in the BEMC. But the physics analysis and event selection is done on the leading cluster energy, i.e. on the most energetic reconstructed cluster. The trigger efficiency for the final DIS sample must be estimated from the two dimensional distribution, on the scatter plot for the leading cluster energy and the total cluster energy (Fig. 7.7). This is valid mainly for low cluster energies where the influence of the event topology can be seen. For energies $E_{CL} > 10\,GeV$ the 1-dimensional functional dependence on the leading cluster energy turns out to be a good approximation. If the hadrons accompanying the electron are emitted into the BEMC angular acceptance region, there is some chance that these hadrons will contribute to the trigger cluster energy and so enhance the trigger probability. But as already mentioned the BEMC is an electromagnetic calorimeter with a very pour hadronic energy measurement and the energy depositions from hadrons have large fluctuations. When estimating the trigger efficiency for the total reconstructed cluster energies we see a rather broad transition region (Fig. 7.7) and the full efficiency is achieved only for $E > 15\ GeV$. This can be explained when studying correlation between the leading cluster and the total cluster energy sum. Even if the total sum is above 20 GeV, there are events where the leading cluster has less than 8 GeV. Of course, this kind of events should be very carefully analysed. To have more than $10 - 12\ GeV$ from hadrons in the BEMC is very inprobable.

Trigger Efficiency Crosscheck Events triggered by other subtriggers (BPC, ZVTX, TOF-IA) and simultaneously with some energy deposit in the BEMC were used for the BSET performance crosschecking. The procedure is the same as described in sec.7.1.2 with one additional requirement, e.g. BPC trigger bit was active (Tabl. 7.2). The results are in good agreement with those obtained from the direct efficiency calculations. Only at low cluster energies the efficiency for events triggered simultaneously by tracker triggers is slightly smaller, but this difference is still within the statistical errors.

7.3.5 Monitor Triggers

Monitor triggers are usually triggers with very loose trigger conditions (low energy thresholds or any hit in tracker detectors) giving high rates and therefore they are prescaled. Subtriggers prescaling by a given number n is in hardware achieved by setting a counter to n and decrementing it with each triggered event. The prescaled trigger fires when the n counter has reached 0, which also resets the counter to n for the next cycle. BSET trigger elements EQ1 (1 high energy cluster) or GE1 (1 or more than 1 high energy cluster) monitor the performance of all cluster triggers. The cluster triggers with lower thresholds and without the TOF-VETO ($\overline{TOF}$) requirement monitor the performance of those with higher thresholds. Trigger CL1 monitors the CL2 and CL3, resp. CL2 monitors CL3. Additionally the CL3 serves also as a monitor for very important TOF trigger. The fraction of good events from the CL3 triggers with a $\overline{TOF}$ signal is used to estimate the number of lost e^-p collisions due to wrong TOF decisions. This found to be less than a few percent.

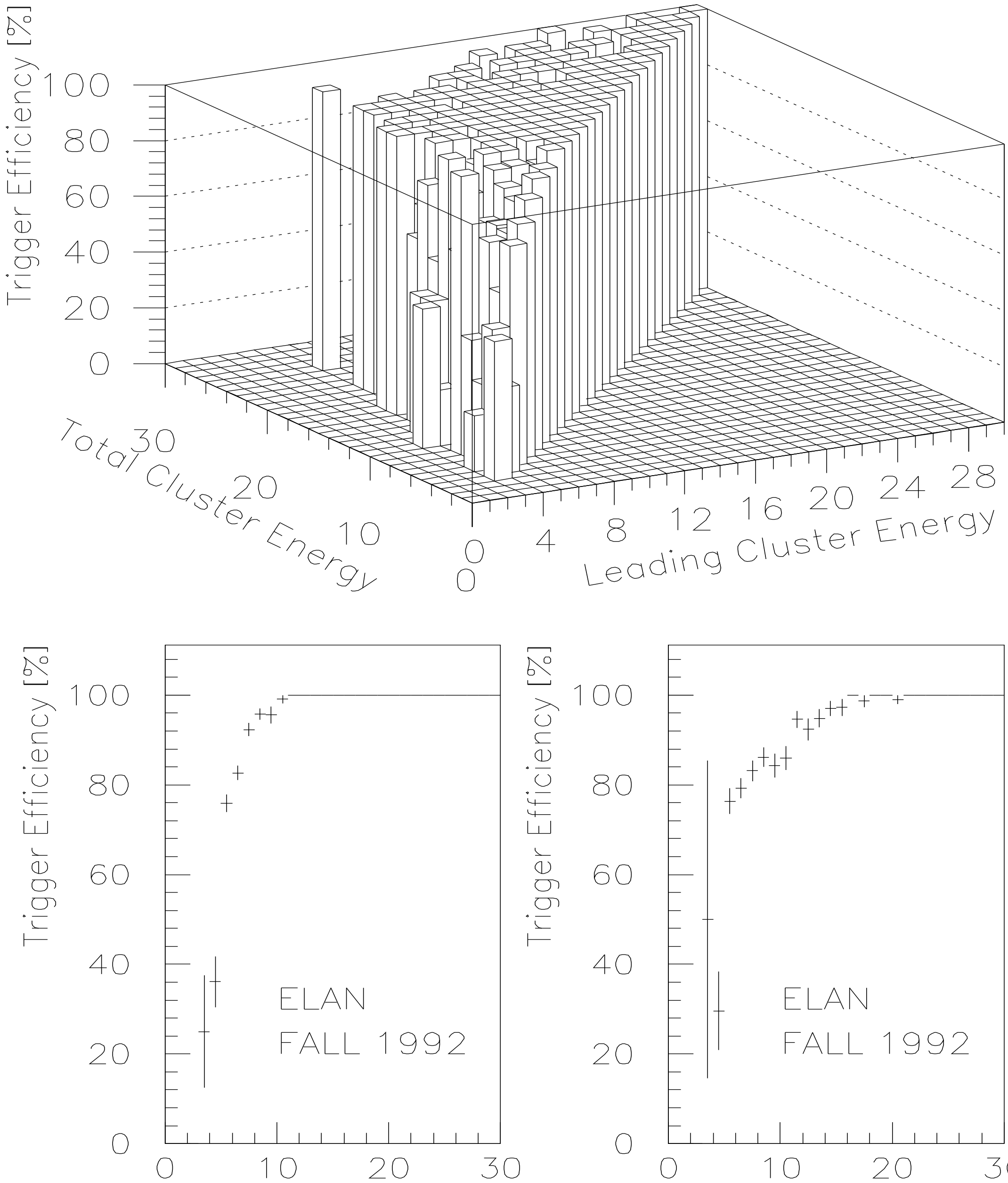

Figure 7.7: *Two-dimensional dependance of the trigger efficiency (a) and projections onto both axis (b,c).*

E(GeV)	Run #, corresponding HT; TCL2 (GeV)				
	all	< 32097	$32097 - 32601$	$32602 - 34533$	> 34533
	mixed	3.6; 3.5	3.2; 3.5	2.8; 3.5	2.3; 2.0
4 - 5	36.1± 5.7	23.1±11.7	25.0±21.7	18.2± 6.7	72.7± 9.5
5 - 6	75.9± 2.0	68.6± 4.3	64.6± 6.9	73.2± 3.1	95.0± 2.2
6 - 7	82.6± 1.6	74.8± 3.9	69.4± 5.9	84.8± 2.4	92.5± 2.3
7 - 8	92.3± 1.5	85.9± 3.9	85.7± 6.6	94.1± 1.9	98.5± 1.5
8 - 9	95.8± 1.3	89.8± 3.9	93.5± 4.4	99.0± 1.0	97.7± 2.3
9 -10	95.6± 1.9	91.2± 4.9	93.3± 6.4	97.8± 2.2	100.0
10 -11	99.1± 0.9	96.7± 3.3	100.0	100.0	100.0
11 -12	100.0	100.0	100.0	100.0	100.0

Table 7.1: *CL2 trigger efficiencies for the leading cluster in the BEMC. Different run periods with different stack (HT) and cluster thresholds (TCL2).*

E(GeV)	Run #, corresponding HT; TCL2 (GeV)				
	all	< 32097	$32097 - 32601$	$32602 - 34533$	> 34533
	mixed	3.6; 3.5	3.2; 3.5	2.8; 3.5	2.3; 2.0
4 - 5	34.8± 5.7	25.0±12.5	25.0±21.7	18.2± 6.7	70.0±10.2
5 - 6	75.8± 2.0	68.4± 4.3	64.6± 6.9	73.1± 3.2	95.0± 2.2
6 - 7	82.7± 1.6	74.6± 3.9	68.9± 5.9	85.4± 2.4	92.5± 2.3
7 - 8	92.3± 1.5	85.9± 3.9	85.7± 6.6	94.1± 1.9	98.5± 1.5
8 - 9	95.8± 1.3	89.8± 3.9	93.5± 4.4	99.0± 1.0	97.7± 2.3
9 -10	95.5± 2.0	90.9± 5.0	93.3± 6.4	97.7± 2.3	100.0
10 -11	99.0± 0.9	96.6± 3.4	100.0	100.0	100.0
11 -12	100.0	100.0	100.0	100.0	100.0

Table 7.2: *CL2 trigger efficiencies for the leading cluster in the BEMC crosschecked by the BPC trigger. Different run periods with different stack (HT) and cluster thresholds (TCL2).*

7.3.6 Pileup

Due to the high rates of background events, *pile-up* effects in the readout electronics chain (preamplifiers, line-drivers, shaper amplifiers) are expected. The pile-up is most critical in the shape amplifier, because this could lead to the wrong energy measurement. Unipolar shape amplifiers ($FWHM = 500\ ns$) used in the BEMC analog electronics are sensitive to the pile-up effects in a time interval of 1 μs, approximately 7 BC before and 3 BC's after the nominal BC [78].

The extended readout of the BSET trigger enables to write into the BSET bank data on the trigger bits status from 32 HERA bunch crossings. This readout mode was used only in the very beginning of the data taking and later was replaced by the compact readout mode, in which only 5 BC were written into the BSET bank. The compact readout mode is used in order to reduce the data volume and consequently DAQ dead-time in the calorimeter branch. The speed and the timing precision of the BSET allows to identify the pileup in the readout chain. In the trigger chain some of elements are fired not only in the nominal BC but also outside this position.

For the unambiguous identification of a pileup the information from another detector with a good time resolution and space correlation is needed. BPC and TOF detectors are potential candidates, but due to the fact that BPC detector information was spread out over 3 consecutive bunches, the unambiguous pileup detection was not possible with this detector. This is true mainly for LTs, called also noise threshold. If the stack above HT has fired outside the nominal BC, the probability is much higher that the reason was real pileup. The pileup probability is inversely proportional to the distance from the beam axis and the highest rate is expected in the innermost triangular stacks. However these stacks were excluded from the trigger as a potential cluster initiator (i.e. HT set practicaly to infinity) and therefore the fraction of events with an additional stack above HT outside the nominal BC position is very small. ($< 1\%$).

When running at $100\times$ higher beam currents pileup problems may become much more serious.

7.3.7 One Diode (1-D) Events

An unexpected type of background events triggered by BSET triggers was found in the data. Unphysical energy sharing between diodes of one stack is a typical signature for them. In these events the stack energy is concentrated only in 1 diode, all others together see only few percent of the stack energy! (Fig. 7.8a). To study this phenomenon we have defined a variable DR as a ratio of the energy seen by the hottest diode in the leading stack to the total stack energy. Cut $DR > 0.95$, later $DR > 0.8$ was used for the rejection of these events on the L4 filter farm.

The radial dependence of the rates (Fig 7.8c) and the correlation with beam currents are a clear indications that source of 1-D events is directly related to the e^-p beams. Synchrotron radiated γ particles and particles from the proton induced background showers hit the diode directly and create the unphysical energy distribution with unknown energy scale. From all 1-D events more than 97 % have only one stack above HT (but remember that the innermost triangular stacks are excluded from the trigger!). To identify the source of these events the so-called p, resp. e^- pilot bunches, i.e. the bunches without its corresponding counterparts, were used. For electron pilot bunch events $\sim 70\%$ of the GE1 triggered events are of the 1-D type ($DR > 0.8$), while from the proton pilot bunch for events not vetoed by the TOF, this number is only 30%. An empty detector with only 1 BEMC stack (1-diode) energy above HT is a typical signature for e^--pilot bunch events, whereas from the proton pilot bunch events more BEMC stacks are hit with a typical signs of the proton induced background. In some cases beam hallo μ are seen and triggered by the muon and/or VETO WALL system.

About $70 - 90\,\%$ of all BSET triggered events rejected on L4 are 1-D events. It is however desirable to get rid of them already on some of the earlier trigger levels, preferably on the L1. The studies on the real data shows that the L1 or L3 trigger rates reduction by a factor ~ 5 is achievable.

Using of single diode signals require major hardware changes (up to now the stack energy = sum of 4 diodes is the smallest available L1 trigger element), but the advantage would be the independence from the other detectors.

Another solution could be a requirement for BSET-BPC spatial correlation. For this purpose we have modified the reconstruction code the same way as in the simulation (see page 59). Matching of the BEMC stacks with the BPC strips and number of required matching BPC planes is defined by the look-up tables. Demanding 3 out of 4 planes (3/4) or 2/4 85 %, resp. 80 % of 1-D events could be recognized and vetoed already on L1 or L3 trigger level. The fact that so many 1-D hit stacks have no corresponding BPC hits indicates that these events are most probably related to the synchrotron radiation.

The solution of this problem becomes more urgent with the higher beam currents. Without significant increase of BSET thresholds the rate of CL2 trigger could be kept at a few Hz level, if 1-D events would be rejected already on L1.

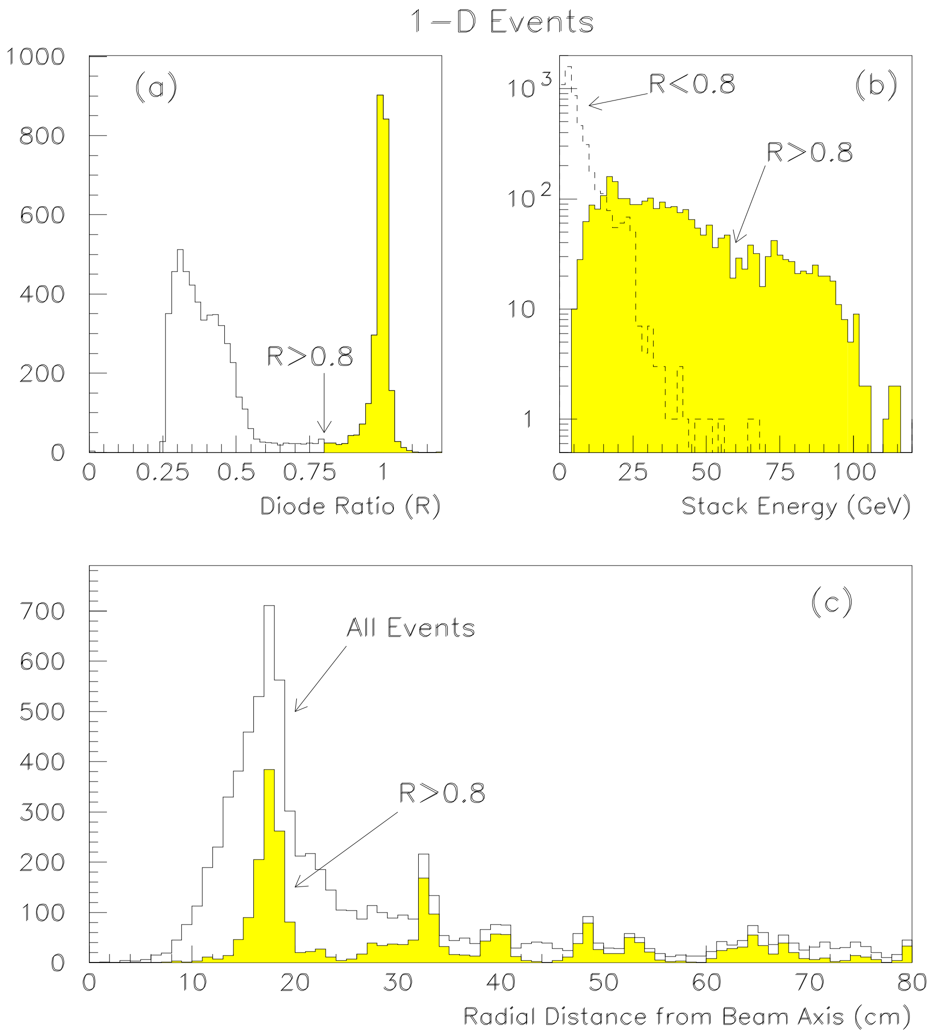

Figure 7.8: *(a) Fraction of the energy seen by the hottest diode in the leading stack. (b) Energy spectra of both events classes. (c) Radial distance of the cluster center of gravity for all and for 1-D events.*

Chapter 8

Measurement of NC DIS at Low Q^2

8.1 Standard Event Selection

The selection of deep inelastic scattering event candidates starts already on the trigger level. There we relied on the BSET cluster trigger CL2 in coincidence with TOF-veto ($CL2 * \overline{TOF}$). The CL2 selects electron candidates in the BEMC and the TOF-veto, on the basis of time information, rejects dominating beam induced background events.

Most of 1992 the HERA machine operated in the 10 + 10 bunch mode at $\sim 1\%$ of the design luminosity. Nevertheless the trigger rate was strongly dependent on the beam conditions and during the data taking period in the autumn 1992 the $CL2 * \overline{TOF}$ rate varied between $1 - 5\ Hz$. Raw rates of the CL2 trigger element without TOF-veto were $\sim 10 - 20\times$ higher.

The second step in the 1992 data events selection is done on the L4 trigger level where the software farm, by applying a set of different cuts using information from all subdetectors, acts as an effective filter. The reduction factor resulting from the two cuts provided by the TOF-veto and the L4 filter varies between $\sim 40 - 100$ (Fig. 8.1). Most of the $CL2 * \overline{TOF}$ triggers ($> 80\%$) are on L4 recognized as 1 diode events (see previous chapter). This is the most serious, partially unexpected source of background events.

From all events which passed L1 and L4, i.e. not only those triggered by CL2, a further DIS selection is done off-line. All reconstructed events written on the production output tape (POT) are classified according to different event classes [64]. An event is classified as a NC DIS low Q^2 candidate if at least one reconstructed energy cluster in the BEMC $E_{BCLR} \geq 4\ GeV$ was found with a BPC hit in the cone of 15 cm around the reconstructed cluster center of gravity. A basic sample (called ELAN miniDST) which is used in the last analysis step containes $\sim$ 8200 NC events candidates and is selected according the following criteria:

- $E_{BCLR} \geq 6\ GeV$
- for cluster energies between $6 - 22\ GeV$ the existence of the central or forward vertex is required
- TOF cut - if there is at least one hit in the physical time window not more than 2 hits in the background window are allowed
- Beam pipe cut - center of gravity of the leading cluster is outside the innermost triangular stacks: $|x_{cog}| > 14\ cm$ or $|y_{cog}| > 14\ cm$

For the final data selection procedure, providing 1019 NC DIS events with $Q^2 < 100\ GeV^2$ (Fig. 8.3a), some of the previous cuts were refined and also additional cuts were made:

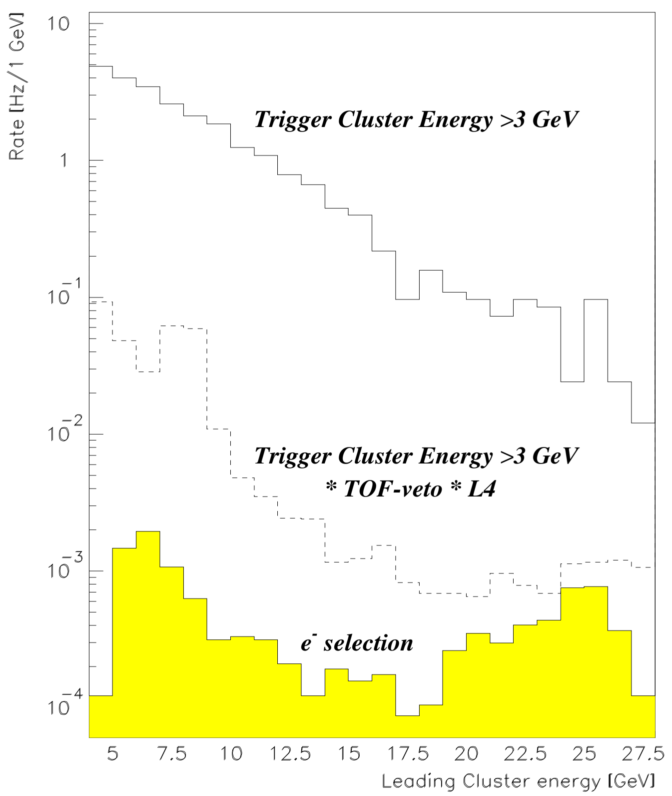

Figure 8.1: *Absolute trigger rates in the BEMC as a function of leading cluster energy at different trigger and reconstruction levels.*

- the spatial correlation between the BPC hit and the BEMC leading cluster center of gravity was refined from 15 cm to 5 cm
- the lateral size (radius) of the cluster was required to be < 5 cm
- the event had to be triggered by the BSET CL2 trigger
- the fraction of good tracks - events with large fraction (> 0.25) of tracks pointing outside the interaction region were rejected
- the vertex reconstructed from tracks in the central tracker was required to be within ± 50 cm from the nominal interaction point ($z = 0$ cm)
- $0.05 < y_e < 0.6$, cut for the analysis based on the electron measurement
- $y_h < 0.5$ cut for mixed analysis only (i.e. both electron and hadrons measurements were used)

The energy E_e and polar angle θ_e spectra of the scattered electron used in the analysis are shown in the Fig. 8.2. The energy spectrum is before the cut on the cluster radius, which rejects mainly the γp background at low energies. For the angular distribution an additional cut on the scattered electron energy $E_e > 10.4\ GeV$ is applied. The shape and the position of the characteristic peak in the E_e distribution near the electron beam energy are only weakly dependent on the MC input structure function. This is used for the electron energy measurement calibration. The achieved precision of the absolute energy scale determination is about 3 %.

The MC events have been generated with the DJANGO 1.0 [65] generator which is an interface between HERACLES [66] and LEPTO [67] generators. HERACLES simulates electroweak interaction with included first order radiative corrections and LEPTO takes into account the QCD processes and parton fragmentation. MC distributions, based on the $MRSD^-$ parton densities [68], are normalized to the integrated luminosity 22.5 nb^{-1} of the measured data sample.

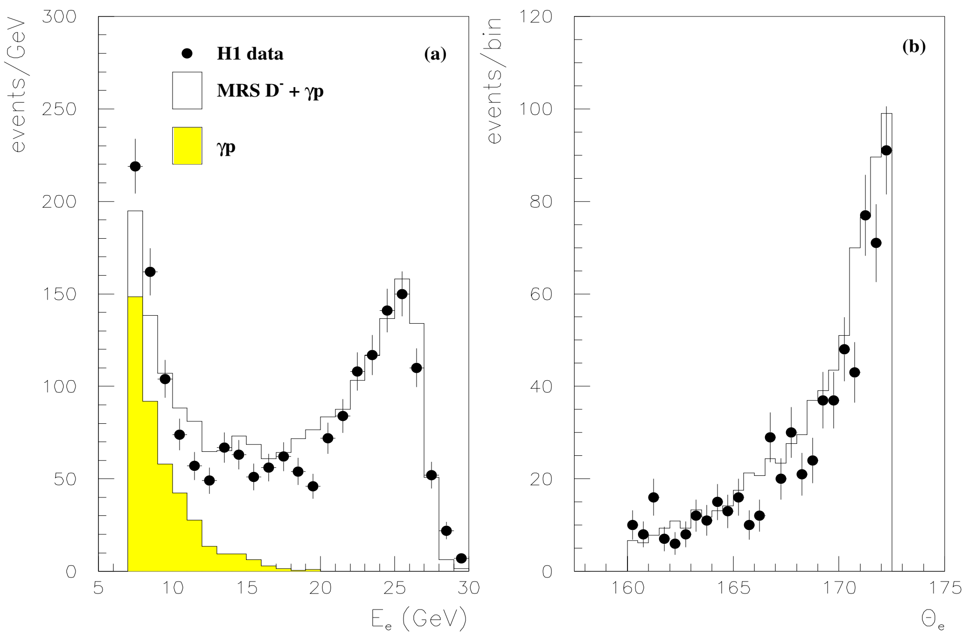

Figure 8.2: *(a) Energy spectrum of the scattered electron before cut on the cluster radius. (b) The electron scattering angle spectrum after additional cuts on the lateral cluster size and on the electron energy $E_e > 10.4\ GeV$.*

8.1.1 Background Subtraction

- **Physics Background** - the most important source of background to the NC DIS events, mainly at high y ($y > 0.6$) is photoproduction (γp). For these events the electron remains in the beam pipe and hadrons and photons produced can mimic a scattered electron in the BEMC.

The number of γp events contaminating the NC DIS sample was determined from the combined analysis using the measured data and the Monte Carlo simulation. To generate hard and soft processes at $Q^2 \sim 0$ the MC event generators PYTHIA [70] resp. RAYVDM [71] were used. The energy spectrum of fake electron candidates falls rapidly with increasing energy (Fig. 8.2). The cut on $y < 0.6$, equivalent to the cut on electron energy $E_e > 10.4\ GeV$, strongly reduces the remaining background in the studied sample. Another effective cut is the 5 cm cut on the radial size of the BEMC cluster. The photoproduction contamination was estimated to be less than 30 % at $E_e = 10.4\ GeV$. Below $y \leq 0.4$ the γp background can be neglected. The residual contamination of the measured x, Q^2 bins was subtracted statistically.

- **Machine Background** - the fraction of events from beam related background surviving the event selection criteria was estimated from the proton and electron pilot bunch events. The upper limit of remaining beam induced background was estimated to be at most 1% in the whole kinematical region [36].

8.2 Discussion

The precise structure function measurement is not a simple task. It requires a very detailed understanding of all systematic errors which could have an impact on the final results. Some effects could be neglected in the first round of measurement when the total systematic errors are still at the $10 - 30$ % level. The knowledge of the absolute energy scale and the energy resolution are the basic ingredients of this tedious process. The electron energy measurement in the BEMC can be affected by two effects which are not taken into account in the current procedure:

- the pileup events
- the events with 1-diode signature in any of the stacks contributing to the cluster energy sum

In this section we want to discuss these effects which could be important in the future when a better understanding of the whole detector will enable to decrease the overall systematic errors down to a few percent level.

- **Pileup Event Candidates** The HERA beam crossing rate of 10.4 MHz means that every 96 ns interactions can occur. As the BEMC readout electronics is much slower, the energy measurement can be deteriorated by the superposition of the signals belonging to the previous 7 or to the subsequent 3 bunch crossings [78]. The identification of these events is possible due to the very good time resolution of the BSET trigger and due to the fact that in the trigger readout the status of all trigger bits (including stacks LT, HT) before and after the triggered event is available.

  In the leading cluster we were looking for the stacks which have their trigger information (low and/or high threshold bit) active outside the nominal BC position. Here we have found two types of events:

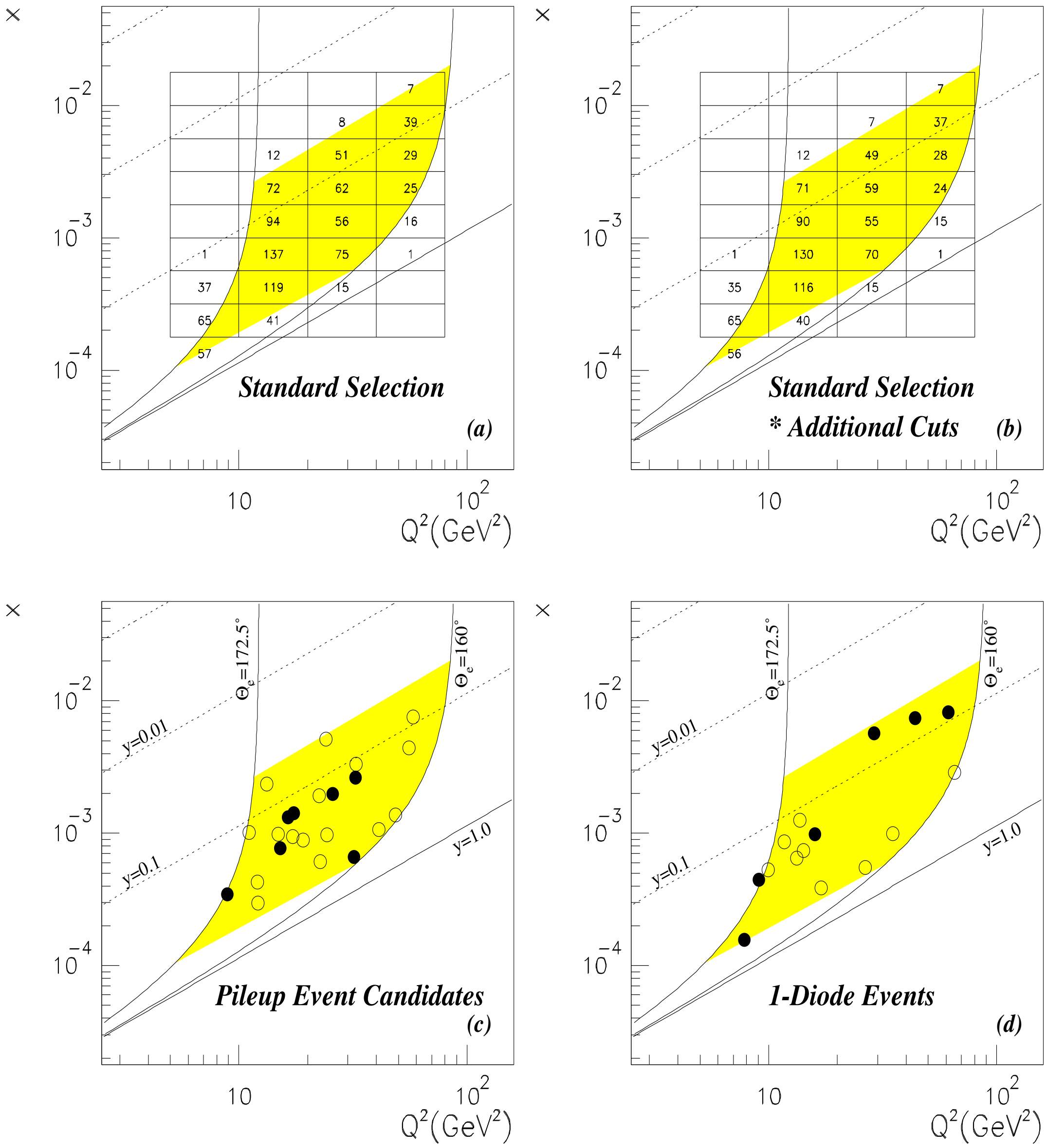

Figure 8.3: *(a) Number of events in the defined bins after standard cuts applied on the preselected sample. (b) Number of events in the same bins after additional cuts, using the time history information of the BSET trigger bits (pileup candidates) and rejecting events in which any stack in the leading cluster had the 1-diode signature. The distribution of pileup event candidates (c) and of 1-diode events (d) in the measured region. With black dots are in both cases marked the events in which the affected stack contained more than 2 GeV.*

  - *primary pileup* - trigger bit is active in the nominal and also in some previous or later BC
  - *secondary pileup* - the stack trigger bit is active only outside the nominal BC

  The events with *primary pileup* should be removed from the final sample, because a proper correction of the measured energy is not possible in this case. For the *secondary pileup*, in the case that energy in the hit stack is not very big (thus the leakage into the adjacent stacks is small), one could try to leave out this stack from the cluster reconstruction algorithm.

  In the ELAN miniDST from summer 1992 and in the final sample after standard selection we have found 3.0 % resp. 2.2 % events which are considered as pileup candidates. In most of these events the energy measured in the hit stack is close to the stack low threshold ($\sim$ 1.3 GeV) and therefore they could be simply noise triggers, without any measurable effect. But in $\sim$ 32 % of these events the energy in the affected stacks is above 2 GeV. The residual fraction of the cluster energy $E_{res} = 1 - (E_{clus} - E_{stack})/E_{clus}$, which could be wrongly measured varied between $\sim 5-15$ %. Unambiguous identification of the real pileup would be possible only with the help of the BPC and/or TOF detectors. Unfortunately the timing adjustment of the BPC, which is intrinsically very fast ($\sim$ 50 ns), was not perfect and the needed information was spread in up to 3 BC. Almost all pileup event candidates are *secondary pileups* and only in 3 cases we can talk about the *primary pileup*. But in this case the affected stack contains rather big fraction of the cluster energy.

- **1-Diode Events** The so-called 1-D events causing the triggering problems were discussed in the previous Chapter 7 (page 97). Events with 1-D signature are normally rejected already on the L4 filter farm and later also in the standard analysis procedure. But in both these steps only the "hottest" stack in the leading cluster was tested. We have checked all stacks contributing with at least 500 MeV to the cluster energy sum and have found that in the ELAN miniDST still $\sim$ 6.2 % of 1-D events were present. In the final sample used for the F_2 structure function measurement still $\sim$ 1.5 % of all events had the 1-D signature (Fig. 8.3 d). It means that for $\sim$ 1.5 % of events the cluster energy measurement could be deteriorated by the contribution from these stacks due to the unphysical energy sharing between the diodes. Although the considered stacks were non-leading ones, the effect on the final energy determination varied between $\sim 5 - 10$ %, with indication of possible tails in the residual energy distribution (two events with 16 % resp. 33 %).

- **Conclusions** Detailed studies of the above mentioned effects have shown, that the fraction of good events affected by the "pileup" or by the existence of 1-D stacks in the leading cluster (Fig. 8.3) is of the order of < 4 %. The impact on the 1992 data with rather big systematic errors ($10 - 30$ %) is negligible. But in the future at $\sim 100\times$ higher luminosity the pile-up probability and the fraction of 1-diode stacks in the BEMC electromagnetic cluster could be larger by factor ~ 5. With better understanding of all systematic effects and reducing them down to a few percent level, the size of the contribution from these two additional sources must be understood and correctly taken into account. Important prerequisite is the precise timing adjustment of all involved detectors (BPC, TOF, BEMC), which are intrinsically very fast. The unambiguous detection of the proper bunch crossings must be achieved.

Summary

- **BSET Trigger** A first level single electron trigger, using stack energy as a basic trigger element, has been designed and built for the H1 backward electromagnetic calorimeter. The trigger is capable to recognize cluster topologies and to set thresholds on the cluster and total energies. The trigger decisions can be uniquely assigned to the correct bunch crossing. The history around the nominal trigger position can be recorded via a digital pipeline.

  The trigger was operated successfully at the first H1 data taking period at HERA and has been a major contributor for the collection of the NC DIS event sample.

- **NC DIS Triggers** Efficient trigger algorithms and various alternatives for triggering of the NC DIS events at $Q^2 < 100\ GeV^2$ based on the H1 trigger simulation results were proposed and used during the data taking at H1. It is shown that in fact with a few subtriggers, as e.g. with the following ones, the whole kinematical region of interest could be effectively covered:

$CL2 * \overline{IST} * \overline{TOF}$	- low Q^2, low y trigger
$CL1 * \overline{IST} * DC - R\phi - thr0 * \overline{TOF}$	- low Q^2, high y trigger
$BTOT * TOF - IA * \overline{TOF}$	- low Q^2, high y trigger
$LAr - Electron * \overline{TOF}$	- high Q^2 trigger

- **Beam Wall, Beam Gas Background** The total background rates at H1 are lower by factor $2-5$ [79] than the predicted ones. On the other hand in the BSET trigger is this partially compensated by the unexpected high rate of 1-diode events originating mainly from synchrotron radiation.

  An algorithm to reject 1-diode events, based on the BPC - BEMC spatial matching, was proposed for the L3 resp. L1 trigger level. The advantage of this solution is that it does not require major hardware changes, but on the other side the rejection efficiency strongly depends on the performance of the BPC. A more reliable solution would be to use the diode signals directly on the L1. In this case major hardware changes are inevitable.

- **Calorimeter Triggers Performance**

  On-Line Monitoring Software to monitor on-line the performance of the BSET and LAr calorimeter triggers was written and implemented on the calorimeter μVAX cluster.

Off-Line Analysis Methods to calculate the trigger efficiency of the BSET trigger for the NC DIS at low Q^2 and techniques to crosscheck the performance of this trigger were elaborated. The cluster trigger worked very reliably and was fully efficient for the energies above 10 GeV.

- **NC DIS Measurement at Low Q^2** On the top of standard ELAN cuts the additional ones, using more detailed trigger information and careful check of all stack energies contributing to the electron cluster, were applied. It was found that fraction of good events, i.e. those selected by the standard criteria, affected by the pileup or 1-diode stacks is of the order of a few percent (< 4 %). These events can be left out from further analysis. When taking into account the achieved precision of the F_2 structure function measurement ($\sim 10 - 30$ % systematic errors), this has a negligible impact on the 1992 data. But in the future at $\sim 100\times$ higher luminosity the pile-up probability and the fraction of 1-diode stacks in the leading BEMC electromagnetic cluster is expected to be $\sim 5\times$ larger. Therefore these effects must be carefully studied. In order to identify the pileup event the information from the BPC and/or TOF detectors has to be used. For this purpose the precise timing adjustment of the involved detectors must be done and the unambiguous detection of the proper bunch crossings must be achieved.

- **Low (x, Q^2) Physics at H1 in the Future** First measurements of F_2 structure function at very low (x, Q^2) would not be possible without a dedicated very efficient electron trigger in the backward region of the H1 detector, without the BEMC calorimeter and without the backward proportional chamber (BPC). But in order to use the full potential of the HERA machine at *very low* (x, Q^2) further improvements in tracking, energy measurement and triggering in this region are needed. They are subject of the H1 upgrade program [83]. From the trigger point of view the improvements are needed in order to:

  - reduce the background rates
  - extend the acceptance in the $\theta - y$ plane
  - provide a redundancy for the low Q^2 trigger acceptance

Appendix A

The H1 Simulation Programs

A.1 The H1SIM Package

The H1 detector simulation program H1SIM is based on two software packages widely used in the high energy physics community, namely: the GEANT3.13 system of the detector description and simulation of particles tracking through the detection media [80], and the BOS77 system for the dynamic memory management [81].

The whole physics of the particles interactions in the detectors (tracking in the electromagnetic field, cross sections, secondary particles generation, shower development) is in H1SIM simulated by the GEANT3.13, but the ZEBRA based I/O part of GEANT is replaced by BOS77.

The modular form of the H1SIM program [59] enables to process only some specific part of the H1SIM. Thus e.g. trigger studies can be done without redoing the time consuming GEANT or DIGI steps.
The H1SIM modular structure is built up from the following main modules:

- *H1GEA*
- *H1DIGI*
- *H1TRIG*

The *H1GEA* module is the main part of the simulation. H1 detector geometry is built in with many fine details resulting in a very realistic detector response ('close to real life'). The negative effect of this approach is a large CPU-time consumption. The input to the GEANT module are *generated events* (particle 4-vectors) and the output are so called *hit banks*, which contain the xyz-coordinates of entry and exit points of the particle trajectories for the sensitive detector parts in the tracking part and energy depositions for calorimeter type detectors.

For a given detector geometry a decisive factor influencing CPU-time consumption are cuts used for the tracking of all particles through the experimental setup. For each calorimetric medium one has to find the optimal cuts which allow correctly describe the fluctuations in the shower development (energy resolution). For the different tasks were in the H1 defined three sets of cuts. For the simulation of electromagnetic showers in the BEMC the medium set ($CUTGAM = 0.2$, $CUTELE = 1.0\ MeV$) of the standard H1 tracking cuts was found as a good compromise [77]. Finer cuts on kinetic energy of photons resp. electrons ($CUTGAM = 0.05$, $CUTELE = 0.1\ MeV$) give the same energy resolution as the medium ones but the time needed to process 1 event is almost 3 times longer (105 ns compared to 38 ns on the DESY IBM 3090-30S). The energy resolution for the first set of cuts (0.2, 10 MeV) was found almost 2× worse then the measured one and therefore not suitable for the precise detector response simulations.

The *H1DIGI* module, which is also H1 specific and not the standard GEANT module, transforms the *hit banks* into the *digi banks*, which contain the detector response in a format similar to real events (channel numbers, wire addresses, ADC counts etc.).

Finally the *H1TRIG* module using the *digi banks* as input creates trigger response BOS banks and combines the single trigger elements into the final trigger decision the same way as it is done in the L1 hardware.

All steering options of the H1SIM detector simulation program are entered via the BOS text banks. The banks are read in from standard input at the beginning of the job. All steering banks are collected inside the text bank OSTX, which itself is contained in a normal textfile. Therefore the user can change any of the steering variables by using the local editor.

In addition to the steering banks there are a lot of *parameter banks*. Typical examples of *parameter banks* contain calibration constants, weighting functions, smearing and resolution parameters, trigger thresholds, noise values etc.

All the parameter banks are managed by the H1 database management system *MDB* [82].

A.1.1 BSET Trigger Code in H1SIM

BSET trigger simulation is part of the *H1TRIG* module and the calling sequence is:

BCTRES
BCTRIG
  BTCLUS
    BTIDEN
      BTCLAD

BCTRES : In this module all thresholds and noise values from the text bank BTTX (BSTH resp. BTNS) are read in. Visible energy from the BRCE digi bank is converted to the real (calibrated) energy. Trigger banks BTTT and BTBT (LAr trigger part trigger towers, resp. big towers) and BTST trigger bank are created. BTST contains BEMC stack numbers and energy depositions in the total and in the backward part of the single stack. Only stacks with energy above Low Threshold (LT) are considered. These stacks are the basic BEMC trigger elements on which the cluster search algorithm works.

BCTRIG : BEMC trigger response is analysed and hardware like BSET bank (B32 format) is created.

BTCLUS : cluster analysis on the BEMC stacks is done

BTIDEN : cluster identification is done

BTCLAD : cluster counting is done. A chain of 2 adjacent hits (stacks above LT or HT) is considered as 1 cluster, 3 or 4 adjacent hits in the row or in the column are considered as 2 clusters and if more than 4 hits are found, simply the number of hits is counted as a number of clusters. It has no sense to calculate exactly the number of clusters, because the $[X, Y]$ projection method exactly determines only 1 cluster and can say that there were 2 or more clusters.

BTTX (BTNS) parameter text bank: σ of the noise in the stacks (total, backward) and in the trigger towers is defined

BTTX (BSTH) Following parameters in this text bank has to be defined:

- 3 (resp.2) thresholds for each stack
  - low threshold for the whole stack
  - high threshold for the whole stack
  - low threshold for 'hadronic' part of the stack
- 3 cluster thresholds
- 1 threshold for the total BEMC energy
- number of hit stacks in the innermost "ring" on both, high and low energy levels
- RATIO parameter defining acceptable leakage from the e^- showers into the 'hadronic' part

Stack thresholds can be all the same or one can redefine some or all low (total) and high thresholds. Excluding the stack from the trigger can be done by setting the corresponding threshold to the unrealisticaly high value.

The number of hit stacks in the innermost ring, mainly on the high energy level, can help to suppress background events rate.

For simulation studies one can use also the RATIO parameter, which is fraction of the energy seen by the so called "hadronic" WLS from the total cluster energy. In the hardware is this feature not realized yet. The main problem comes from fluctuations of the leakage into the backward part, even from electrons, and from the relatively large noise in this part of the calorimeter.

A.2 The H1FAST

This fast, but still accurate shower parametrization is included into the GEANT framework and can be used alternatively to the detailed shower simulation.

The sampling structures of the H1 calorimeters are replaced by homogeneous volumes filled with averaged media. Energy depositions simulated in these media are mapped onto the actual read out geometry. The signal (e/mip, e/h effects) and the desired resolution are generated in a second step by applying external response functions.

In the electromagnetic shower parametrization [74] the longitudinal and lateral shower shapes as well as their fluctuations and correlations are simulated.

In the hadronic showers only electromagnetic subshowers in the cascade are being parametrized. Parametrization over cracks is not allowed because it cannot be easily parametrized and this leads to an incorrect description of the energy losses in the dead material [73].

The fast MC is implemented in the general framework of GEANT for geometry description and particle tracking, while GHEISHA or FLUKA produce hadronic interactions.

All energy depositions (e.m., hadronic, energy lost in a nuclear reactions) in all parts of the detector are stored in BOS banks. This allows to reconstruct the response after simulation with simple response functions, which are basically sums over the smeared true energy depositions [75],[76]. This scheme provides the possibility of quick retuning with different response functions, and in addition the absolute energy scale of the MC is intrinsically correct.

A.3 The H1PSI (Parametrised Simulation)

A.3.1 BEMC Geometry in H1PSI

The whole geometry description of the H1 detector is simplified in the H1PSI program. Many details are left out and material properties are averaged. Main differences in the BEMC description between H1PSI and H1SIM are the following:

- projective geometry in H1PSI with 5 Θ and 16 ϕ bins
- different granularity, in addition H1PSI BEMC stacks' size is radius dependent, most striking is the difference in the innermost ring where 4 H1PSI stacks correspond to 1 H1SIM stack
- different number of basic trigger elements (H1PSI 80 and H1SIM 88 stacks)
- angular acceptance - H1PSI ($154° - 176°$), H1SIM ($150.6° - 175.6°$)
- in H1PSI is the 'hadronic part' of the stacks missing

A.3.2 BSET Trigger Code in H1PSI

Calling sequence:

```
BTGINI
CATRES
    BTRING
BSTRIG
    BTCLUS
        BTIDEN
            BTCLAD
```

BTGINI : In this module all thresholds and noise values from the text bank BTTX (BSTH resp. BTNS) are read in.

CATRES : The calibrated energy from the CACE digi bank is read out and BEMC channels are renumbered to 1 - 80. Numbering is spiraling from outermost ring and stops in the innermost ring. Depositions in the innermost ring are reorded due to the already mentioned difference in the granularity. Energies in the four adjacent stacks are summed up and put into the stack with maximal original deposit. If the corresponding steering parameter is chosen, noise is added to each stack.

Trigger banks UATB, UBTT and UBTB (LAr trigger part trigger towers, resp. big towers) and UBTS trigger banks are created. UBTS contains BEMC stack numbers and energy depositions in the whole stack. The so called hadronic part does not exist in H1PSI. In a similar way as in H1SIM only stacks with energy above LT are considered. These stacks, as in H1SIM, are the basic BEMC trigger elements on which the cluster search algorithm works.

BSTRIG : the BEMC trigger response is analysed and BSET trigger bits are stored in the TRBEMC common.

BTCLUS : the cluster analysis on the BEMC stacks is done, but now unlike in H1SIM the $[R, \phi]$ projections are used for cluster search

BTIDEN : cluster identification

BTCLAD : cluster counting is done. For the cluster definition and number of found clusters the same considerations as in H1SIM are valid.

BTTX (BTNS) is the parameter text bank: σ of the noise in the stacks (total, backward) and in the trigger towers is defined

BTTX (BSTH) parameter text bank for which the following thresholds has to be defined:

- 2 thresholds for each stack
  - low threshold
  - high threshold
- 3 cluster thresholds
- 1 threshold for the total BEMC energy

The same way as in H1SIM different thresholds for each stack can be defined. The (R, ϕ) symmetry is also used and the stack thresholds for the whole rings can be changed in one step.

Appendix B

The BEMC parameters

B.1 Material Constants

The basic material constants important for the development of electromagnetic and hadronic showers are summarized in Table 4.1. Mean values for the whole BEMC (last row) of the nuclear interaction length λ_0, radiation length X_0, critical energy E_k and Moliére radius R_M are calculated according the approximate analytical formulae of U. Amaldi [72]:

$$\lambda_0 \simeq 35A^{1/3}\,[gcm^{-2}] \tag{B.1}$$

$$X_0 \simeq 180\frac{A^2}{Z}\;[gcm^{-2}] \quad (\frac{\Delta X_0}{X_0} < \pm 20\% \quad for \quad 13 \leq Z \leq 92) \tag{B.2}$$

$$E_k \simeq \frac{550}{Z}\,[MeV] \quad (\frac{\Delta E_k}{E_k} < \pm 10\% \quad for \quad 13 \leq Z \leq 92) \tag{B.3}$$

$$R_M \simeq 7\frac{A}{Z}\,[gcm^{-2}] \quad (\frac{\Delta R_M}{R_M} < \pm 10\% \quad for \quad 13 \leq Z \leq 92) \tag{B.4}$$

Table 4.1 Material constants

Material	Z	A	ρ $[gcm^{-3}]$	λ_0 [cm]	X_0 [cm]	E_k [MeV]	R_M [cm]
Al	13	26.98	2.70	39.4	8.9	39.3	3.69
Pb	82	207.19	11.35	17.09	0.56	7.2	1.56
Polystyrol	6	12	1.03	79.50	42.40	87.0	14.0
38.5% Pb,61.5% scin.	72.4?	182.6?	4.98	39.8	1.44	8.9	3.55

Table 4.2 BEMC module construction in X_0, λ_0, units

$\#of layers$	Material	Total Thickness in X_0	Total Thickness in λ_0
1	18 mm Al	0.20	0.05
49	2.5 mm Pb	21.88	0.72
50	4 mm SCSN 38	0.47	0.25
		Σ = 22.55	Σ = 1.02

B.2 The BEMC Geometry (Granularity)

Most of the BEMC stacks are of the size $15.9 \times 15.9\ cm^2$. This size includes the complete steel box housing. The active size of the sampling structure is approximately $15 \times 15\ cm^2$. All other exotic types of stacks are not much smaller. This means that granularity is too big if compared to the Moliére radius 3.55 cm characterizing the lateral size of the electromagnetic shower in this medium.

Nonprojective geometry and gaps (cracks) between the stacks are the sources of energy losses in the BEMC fiducial volume and make the task of the electron measurement and triggering more complicated.

Longitudinaly the BEMC stacks are readout from two samples:

- from the whole length of the stack - E_{tot}
- from the last third of the stack - E_{had}

B.2.1 Transversal Size of EM Showers

The lateral size of e.m. shower scales with the Moliére radius R_M, which describes the average lateral deflection of electrons with energy ϵ_c after traversing 1 X_0 and is essentially caused by two effects:

1. due to multiple Coulomb scattering electrons move away from the shower axis
2. bremsstrahlung photons may deflect quite far from the axis, particulary if they are emitted by electrons that themselves travel under a relatively big angle

The first process dominates in the early stages of the cascade development, while the second process is dominant beyond the shower maximum, particulary in high-Z media [84].

$$R_M = X_0 \frac{E_s}{\epsilon_c} \approx \frac{(21.2MeV)}{\epsilon_c} \tag{B.5}$$

Near t_{max} almost all the shower is contained in a core of radius $\sim 1\ X_0$, but deeper in the shower, the core is surrounded by an extensive halo of multiply scattered low energy electrons, such that 95% of the shower energy is contained in a cylinder of $\sim 2\ R_M$. Transversal size or in the terms BEMC trigger elements, number of hit stacks and amount of energy deposited in them tell us what is the cluster size we should use in the trigger (see chapter 5.1.1).

B.2.2 Energy Containment (Energy Leakage)

Electrons The calorimeter length L needed to contain a fixed fraction 98% of the incident particle energy can be computed from the approximate analytical relations [72]:

$$L(98\%) = 3t_{med} \tag{B.6}$$

$$t_{med} = (\ln \frac{E}{E_k} + 0.4) \tag{B.7}$$

where t_{med} is the median depth of the shower, i.e. depth at which half of the initial energy is deposited. In our case it turns out that $L(98\%) = 25.5\ X_0$. If the $10-20\%$ error of this calculation is taken into account, this roughly corresponds to the total BEMC length. Test measurements confirmed that EM showers are well contained even for maximal 30 GeV electrons with negligible leakage behind the BEMC ($\sim 600\ MeV$) [56].

Leakage problems arise at angles above 173^0 (close to the beam pipe) where the electron hits the BEMC near to the edge and part of the energy is lost due to the transversal size of the shower. Due to the triangular form of the innermost BEMC stacks the energy losses are also dependent on the azimuthal angle ϕ.

The second "leaky" area arises at angles smaller than 156^0 (Fig 2.3). In this case BEMC depth seen by the traversing particle is not sufficient for full containment and due to the not projective geometry the side leakage also plays its role of course. Overlap with the liquid argon calorimeter is not very good and big energy corrections have to be applied in this region.

Other areas where some portion of the energy is lost, even in the good angular region, are those in between the BEMC stacks, in the gaps between the basic building blocks.

Quantitative estimates of all these effects and energy sharing between adjacent stacks define the cluster energy thresholds which should be used for well controlled triggering on the defined electron energies.

Hadrons From the similar equations for *hadronic showers* [72]:

$$x_{med} = (0.54 \ln E + 0.4)\lambda_0 \tag{B.8}$$

$$L(95\%) \simeq 2.5 x_{med} \tag{B.9}$$

we realize that the calorimeter length needed to absorb 95% energy of incident 5 and 10 GeV pions is 3.2 resp. 4.2 λ_0.

From these BEMC parameters is clear that BEMC is really only electromagnetic calorimeter, with good containment of electromagnetic showers but too "short" ($\lambda_0 = 1.02$) for hadronic particles.

e^-/π separation achievable with the BEMC alone is insufficient and good e^- identification below 10 GeV is rather difficult. This is very severe for the L1 trigger level, where additional means of the off-line analysis are not available.

Bibliography

[1] ECFA 80/42, March 1980, DESY HERA 80/01,
Study on the Proton-Electron Storage Ring Project HERA

[2] H1 Collaboration, DESY June 28, 1985,
Letter of Intent for an Experiment at HERA

[3] H1 Collaboration, March 1986,
Technical Proposal for the H1 Detector

[4] H1 Collaboration, October 1987,
Technical Progress Report

[5] G.Ingelman, R. Rückl, in Proc. of the HERA Workshop,
Hamburg 1987, Ed. R.D. Peccei, Vol.1, p.107

[6] B. Campbell,V. Elias, W.R. Frisken, Can. J. Phys. 59 (1981) 1742
E. Lohrmann, K.-H. Mess, DESY HERA 83/03 (1983)

[7] M. Klein, PHE 90-25, Zeuthen Preprint, November 1990,
Deep Inelastic Scattering at HERA

[8] J. Blümlein et al., in Proc. of the HERA Workshop,
Hamburg 1987, Ed. R.D. Peccei, Vol.1, p.67

[9] Ed. U. Amaldi, DESY 79/48 (1979), p. 391-394,
Proc. of the study of an ep facility for Europe

[10] J. Feltesse, DAPNIA/SPP 92-01, January 1992, Revised version
HERA the New Frontier, Lectures pres. at the SLAC Summer Institute,
Stanford, California, 5-16 August 1991

[11] G. Bernardi, W. Hildesheim, in Proc. of the Physics at HERA Workshop,
Hamburg 1991, Eds. W.Buchmuller, G. Ingelman, Vol. 1, p.79

[12] S. Bentvelsen et al., in Proc. of the Physics at HERA Workshop,
Hamburg 1991, Eds. W.Buchmuller, G. Ingelman, Vol. 1, p.23

[13] J.D. Björken, Phys.Rev **179**(1969) 1547
J.D. Björken, E.A. Paschos, Phys.Rev **185**(1969) 1975

[14] E.D. Bloom et al., Phys.Rev.Lett. **23**(1969) 930

[15] R.P. Feynman, Phys.Rev.Lett. **23**(1969) 1415
R.P. Feynman, W. A. Benjamin Inc., 1972,
Photon-Hadron Interactions

[16] G. Miller et al., Phys.Rev. **D5**(1972) 528
A. Bodek et al., Phys.Rev.Lett. **30**(1973) 1087

[17] C. Chang et al., Phys.Rev.Lett. **35**(1975) 901
H.L. Anderson et al., Phys.Rev.Lett. **37**(1976) 1034
S. Stein et al., Phys.Rev. **D12**(1975) 1884

[18] A.D.Martin et al., Nucl.Phys.B (Proc.Suppl.) **29A**(1992) 14

[19] P. Amaudruz et al., Phys.Rev.Lett. **66**(1991) 2712

[20] H. Plothow-Besch, CERN-PPE,1992.07.22, W5051 PDFLIB,
PDFLIB: Structure Functions and α_s Calculations, (User's Manual)

[21] L.V. Gribov, L.N. Lipatov, Sov.Journ.Nucl.Phys. **15**(1972) 438 and 675
G. Altarelli, G. Parisi, Nucl.Phys. **126**(1977) 297
Yu. L. Dokshitser, Sov.Phys.JETP **46**(1977) 641 G. Marchesini, B. Webber, Nucl.Phys. **B349**(1991) 617

[22] E.A. Kuraev, L.N. Lipatov, V.S. Fadin, Sov.Phys.JETP **45** (1977) 199
Ya. Ya. Balitzky, L. N. Lipatov, Sov.Jour.Nucl.Phys. **28**(1978) 822

[23] B. Webber, Proc. of the Physics at HERA Workshop,
Hamburg 1991, Eds. W.Buchmuller, G. Ingelman, Vol. 1, p.285
G. Marchesini, B. Webber, Nucl.Phys. **B349**(1991) 617

[24] L.V. Gribov, E.M. Levin and M.G. Ryskin, Nucl.Phys. **B188**(1981) 555; Phys. Rep. **100**(1983)

[25] A. Donnachie, P.V. Landshoff, Phys.Lett. **185B**(1987) 403

[26] A.H. Mueller and J. Qiu, Nucl.Phys. **B268**(1986) 427

[27] J. Bartels, J. Feltesse, Proc. of the Physics at HERA Workshop,
Hamburg 1991, Eds. W.Buchmuller, G. Ingelman, Vol. 1, p.131

[28] A.H. Mueller, Nucl.Phys.B (Proc.Suppl.) **18C**(1991) 125
A.H. Mueller, Navelet, Nucl.Phys. **B282**(1987) 727
J. Bartels et al., Proc. of the Physics at HERA Workshop,
Hamburg 1991, Eds. W.Buchmuller, G. Ingelman, Vol. 1, p.203

[29] M.G. Ryskin, M. Besancon, Proc. of the Physics at HERA Workshop,
Hamburg 1991, Eds. W.Buchmuller, G. Ingelman, Vol. 1, p.215

[30] K. Charchula, E.M. Levin, Proc. of the Physics at HERA Workshop,
Hamburg 1991, Eds. W.Buchmuller, G. Ingelman, Vol. 1, p.223

[31] G. Ingelman, K. Janson-Prytz, Proc. of the Physics at HERA Workshop,
Hamburg 1991, Eds. W.Buchmuller, G. Ingelman, Vol. 1, p.233

[32] G. A. Schuler, in Proc. of the Physics at HERA Workshop,
Hamburg 1991, Eds. W.Buchmuller, G. Ingelman, Vol. 1, p.461
A. Levy, ibid. p.481
S. Levonian, ibid. 499
G.Schuler, J. Terron, CERN-TH 6415/92 (1992)

[33] B. Schremp, in Proc. of the Physics at HERA Workshop,
Hamburg 1991, Eds. W.Buchmuller, G. Ingelman, Vol. 2, p.1034

[34] H1 Collaboration (T. Ahmed, ...T.Kurča...,et al.), DESY-92-160, Nov 1992
Phys.Lett. **B299**(1993) 374-384
Total photoproduction cross-section measurement at HERA energies

[35] H1 Collaboration (T. Ahmed, ...T.Kurča...,et al.), DESY-92-164, Nov 1992,
Phys.Lett. **B299**(1993) 385-393,
Observation of deep inelastic scattering at low x

[36] H1 Collaboration (I. Abt, ...T.Kurča...,et al.), DESY-93-117, Aug 1993,
Nucl.Phys. **B407**(1993) 515-535,
Measurement of the proton structure function $F_2(x, Q^2)$ in the low x region at HERA

[37] H1 Collaboration (T. Ahmed, ...T.Kurča...,et al.), DESY-92-162, Nov 1992
Phys.Lett.**B298**(1993) 469-478,
Measurement of the hadronic final state in deep inelastic scattering at HERA

[38] H1 Collaboration (T. Ahmed, ...T.Kurča...,et al.), DESY-93-029, March 1993,
Nucl.Phys. **B396**(1993)3-23,
A Search for Leptoquarks, Leptogluons and Excited Leptons in H1 at HERA

[39] Ch. Berger at al., in Proc. of the Physics at HERA Workshop,
Hamburg 1991, Eds. W.Buchmuller, G. Ingelman, Vol. 2, p.1029

[40] B. Andrieu et al., DESY-93-078, June 1993,
to be published in Nucl.Instr.& Methods,
The H1 Liquid Argon Calorimeter System

[41] F.W. Brasse, DESY 92-140, Hamburg October 1992,
The H1 Detector at HERA

[42] D. Breton et al., H1 Int. Report H1-04/92-219,
H1 calorimeter calibration electronics

[43] E. Elsen, in Procc. of the International Symposium Electronic Instrumentation in Physics, Dubna, May 14-17, 1991,
H1 note, H1-01/93-262, Hamburg Januar 1993,
The H1 Trigger and Data Acquisition System

[44] P. Loch, PhD Thesis, FH1K-92-02, DESY intern., October 1992,
Kalibration des H1 Flüssig-Argon Kalorimeters unter Berücksichtigung der Gewichtungsmethode für Teilchenjets

J. Gayler, H1 note, H1-10/92-250, DESY, Hamburg, October 1992,
Contr. to the 3rd Intern. Conf. on Calorimetry in High Energy Physics, Sept. 29 - Oct. 2, 1992, Corpus Christi, Texas
Performance of the H1 Liquid Argon Calorimeter

[45] J. Tutas, H1 note, H1-10/92-246, DESY, Hamburg 1992,
The limited streamer tube system of H1

[46] J. Tutas, H1 note, H1-07/91-185, DESY, Hamburg, July 1991,
A Level 1 Trigger from the Limited Streamer Tube system

[47] BEMC Group, H1 note, H1-07/92-233, DESY, Hamburg 1992,
The H1 Backward Electromagnetic Calorimeter

[48] J. Coughlan et al., H1-04/90-135, DESY, Hamburg April 1990,
Proposal to build muon triggers and time-of-flight hodoscope for the H1 experiment at HERA

[49] D. P. Johnson, H1 note, H1-07/87-65, April 1987,
Beam-Gas Background at HERA

[50] G. Grindhammer et al., H1-TR-300, September 1987,
The First Level Liquid Argon Calorimeter Trigger Physics Requirement

[51] R.J. Ellison, U. Straumann, H1 note, H1-05/90-137, May 1990

[52] H. Brettel et al., H1-MPI-140, Munich, October 1990,
Calorimeter Event t_0 and trigger elements for CTL and DSP

[53] J. Bán, T. Kurča, M. Seman, IEP Košice, September 1990,
Proposal for separated electron and independent t_0 trigger for BEMC

[54] H. Krehbiel, DESY, July 1991,
The extended fan out card of the H1 STC

[55] H.T. Duhme et al., H1 note, September 1991,
VME board GPTP - General Purpose Trigger Pipe (User Manual)

[56] BEMC Group, H1 note, H1-08/92-234,
Calibration and Reconstruction of the BEMC

[57] F. Descamps, C. Vallee, H1 note H1-10/92-256,
Data Acquisition for the H1 Calorimeters

[58] S. Levonian, H1 software note 03/91-20,
EVLOOK - An Interactive Program for the H1 Event Display

[59] S. Egli, H1 software note 10/90-12,
BOS modules in H1 software - A set of rules and recommendations

[60] R. Eichler et al., H1 note, H1-4/87-61, H1-TR 302, DESY, April 1987,
The First Level MWPC Trigger for the H1-Detector
S. Eichenberger et al., H1-note, H1-02/92-214, DESY, Februar 1992,
A Fast Pipelined Trigger for the H1 Experiment based on Multiwire Proportional Chamber Signals

[61] Th. Wolff et al., H1-note, H1-02/92-213, DESY, Februar 1992,
A Driftchamber Track Finder for the First Level Trigger of the H1-Experiment

[62] S. Levonian, in Proc. of the Physics at HERA Workshop,
Hamburg 1991, Eds. W.Buchmuller, G. Ingelman, Vol. 1, p.499,
Total Photoproduction Cross Section Measurement at HERA

[63] J. Heatherington et al., H1 note, H1-08/93-307, DESY, Hamburg 1993,
Studies on TOF FTDC data

[64] H. Hufnagel et al., unpublished, H1 internal software information,
L5-Event Classification

[65] G.A. Schuler, H. Spiesberger, Proceedings, Physics at HERA,
Hamburg 1991, Eds. W.Buchmuller, G. Ingelman, Vol. 3, p.1419,
DJANGO: the interface for the event generators HERACLES and LEPTO

[66] A. Kwiatkowski et al., Comp.Phys.Commun. 69 (1992) 155

[67] G. Ingelmann, "LEPTO 5.2", unpublished program manual;
H. Bengtsson et al. Nucl.Phys. **B301**(1988) 554

[68] A. D. Martin et al., Phys.Rev. **D47**(1993) 867

[69] G.A. Schuler, T. Sjöstrand, Phys.Lett. **B300**(1993) 169

[70] T. Sjöstrand in Proc. of the Physics at HERA Workshop,
Hamburg 1991, Eds. W.Buchmuller, G. Ingelman, Vol. 3, p.1405
PYTHIA at HERA

[71] H1 interface program to LUCVDM of the LUCIFER package of
G. Ingelman and A. Weigend, Computer Phys. Comm. **46**(1987)241

[72] U. Amaldi, Phys.Scripta **V23**(1981) 409-424,
Fluctuations in Calorimetry Measurements

[73] M. Kuhlen, H1 internal note H1-10/92-254,
presented at XXVI Int. Conf. on High Energy Physics, Dallas 1992,
The Fast H1 Detector Monte Carlo

[74] S. Peters, PhD Thesis, Universität Hamburg, 1992
Die parametrische Simulation elektromagnetischer Schauer.

[75] M. Rudowicz, PhD Thesis, Universität Hamburg, 1992
Hadronische Schauersimulation für H1-Detector.

[76] G. Bernardi et al., H1 Software Note 26, (1991),
Calibrated Energies in H1 Detector Simulation

[77] P. Reimer, H1/BEMC group internal note No. 10-90,
MC study of BEMC energy resolution and software calibration constant dependence on impact point position, electron energy and ep vertex smearing

[78] BEMC group, H1 internal note H1-08/92-233,
The H1 Backward Electromagnetic Calorimeter (BEMC)

[79] D. Handschuh, PhD Thesis, Universität Hamburg, 1993
Studien zum Protoninduzierten Untergrund am H1 Detektor und Entwicklung von Filteralgorithmen zu dessen Unterdrückung

[80] R. Brun et al., DD/EE/84-1, CERN, September 1987,
GEANT 3

[81] V. Blobel, DESY R1-88-01 Internal Report, Januar 1988,
The BOS System Dynamic Memory Management,
Second updated printing Fortran77 Version

[82] L. Criegee, privat communication

[83] H1 Collaboration, PRC 92/03, H1 09/92-243, DESY, September 1992,
Letter of Intent to Upgrade the Backward Region of the H1 Detector
H1 Collaboration, PRC 92/01, H1 06/92-226, DESY, June 1992,
Technical Proposal to build Silicon Tracking Detectors for H1

[84] R. Wigmans, in Techniques and Concepts of High-Energy Physics VI,
ed. Th. Ferbel, Series B: Physics Vol. 275, p. 325, 1990, St. Croix,
Calorimetry in High Energy Physics

Acknowledgments

First of all I would like to thank the H1 Collaboration and its spokesmen Prof.Dr. F. Eisele and Prof.Dr. J. Feltesse for their encouragement and the possibility to work with H1 at DESY.
I would like also to express my gratitude to DESY and the DFG for their financial support, which enabled my stay at Hamburg.

I greatly appreciate the support from the Directorate and from the High Energy Physics Departement of my home Institute of Experimental Physics in Košice.
I would like to thank all my colleagues in Košice whose contribution enabled me to join the H1 experiment, especially Dr. M. Seman for his suggestion and first ideas on the single electron trigger for the BEMC, the engineers J. Bán, J. Špalek, F. Kriváň who practically realized the BSET trigger ideas and Dr. J. Ferencei for his enthusiastic effort and coordination of the work connected with running of the BEMC and the BSET.

I would like to thank Prof.Dr. K. Meier for his support and his coordination of the BEMC group.

I am very grateful to Dr. A. DeRoeck for his support and many illuminating dicussions about the triggering of NC DIS. It was a great pleasure to work in the H1 trigger group and in the electron physics analysis group ELAN. Discussions with Dr. M. Klein, Dr. Th. Naumann and E. Peppel were very helpful for me. I would like to thank Dr. G. Cozzika, Dr. A. DeRoeck and Dr. E. Elsen for careful reading of the manuscript and for many useful suggestions and comments.

I would like to thank all members of the BEMC group from the I. Institute of Physics at University Hamburg, lead by Prof.Dr. H.-H. Duhm, for their friendship, kind hospitality and help not only at physics related problems. Special thanks to H.-P. Kasselmann for his friendly help during the completion of this thesis and for stimulating discussions.

I am very grateful to Prof.Dr. H.-H. Duhm for motivating discussions, for his kind support and his readiness to take over the supervisor's duties. Many thanks also to Prof.Dr. W. Bartel for his interest and willingness to write the referees report.

Last but not least I would like to thank my wife Viera for her patience and understanding of my almost permanent absence from home.